Properties of the rotational bands in deformed odd-odd ^{184}Au

S. C. Li (李仕成),[1,2] Y. H. Zhang (张玉虎),[1,*] X. H. Zhou (周小红),[1] S. Guo (郭松),[1] M. L. Liu (柳敏良),[1]
B. S. Gao (高丙水),[1,2] G. de Angelis,[3,4] N. Marginean,[3] A. Gadea,[3] D. R. Napoli,[3] M. Axiotis,[3] C. Rusu,[3] and T. Martinez[3]
[1]*Institute of Modern Physics, Chinese Academy of Sciences, Lanzhou, China*
[2]*Graduate University of Chinese Academy of Sciences, Beijing, China*
[3]*Istituto Nazionale di Fisica Nucleare, Laboratori Nazionali di Legnaro, Legnaro, Italy*
[4]*Hahn-Meitner-Institut, Berlin, Germany*
(Received 7 November 2012; revised manuscript received 18 December 2012; published 10 January 2013)

High-spin states in ^{184}Au have been investigated by means of in-beam γ-ray spectroscopy techniques using the multidetector array of GASP. Excited states of ^{184}Au were populated via the ^{159}Tb(^{29}Si, $4n\gamma$) reaction at a beam energy of 140 MeV. The previously known bands based on the $\pi h_{9/2} \otimes \nu 7/2^-[514]$, $\pi h_{9/2} \otimes \nu 1/2^-[521]$, $\pi h_{9/2} \otimes \nu i_{13/2}$, and $\pi i_{13/2} \otimes \nu i_{13/2}$ configurations have been extended. Three new rotational bands have been identified and assigned as the prolate $\pi 1/2^+[660] \otimes \nu 7/2^-[514]$ and $\pi 11/2^-[505] \otimes \nu 7/2^-[514]$ and oblate $\pi h^{-1}_{11/2} \otimes \nu i^{-1}_{13/2}$ configurations, respectively. Experimental aligned angular momenta, band-crossing frequencies, and electromagnetic properties have been analyzed in the framework of the cranked shell model. Low-spin signature inversion has been observed in the prolate $\pi h_{9/2} \otimes \nu i_{13/2}$ and $\pi i_{13/2} \otimes \nu i_{13/2}$ and oblate $\pi h^{-1}_{11/2} \otimes \nu i^{-1}_{13/2}$ bands of ^{184}Au.

DOI: 10.1103/PhysRevC.87.014310 PACS number(s): 21.10.Re, 23.20.Lv, 27.70.+q

I. INTRODUCTION

Nuclei near the $Z = 82$ proton shell closure are known to exhibit shape coexistence [1], which has been extensively investigated both experimentally and theoretically in the isotopes of Pt, Au, and Hg. For Au nuclei with $A < 187$, prolate shapes dominate the yrast states, while the heavier nuclei ($A > 187$) show mainly oblate shapes. The proton Fermi level in Au nuclei lies between the upper $\pi h_{11/2}$ and lower $\pi h_{9/2}$ subshells. For nuclei with prolate shapes the odd proton occupies predominately the low-Ω $h_{9/2}$ and $i_{13/2}$ orbitals and the excitation levels act like particle states, while for nuclei with oblate shapes the odd proton occupies mainly the low-Ω $h_{11/2}$ orbital and the excitation levels act like hole states. Since prolate bands dominate the high-spin level structures in ^{183,185}Au [2,3], ^{183}Pt [4], and ^{185}Hg [5], the two-quasiparticle bands with prolate shapes in ^{184}Au were easily observed by in-beam study [6]. However, one-quasiparticle bands associated with the oblate $\pi h^{-1}_{11/2}$ and $\nu i^{-1}_{13/2}$ configurations have been observed to be low lying in ^{185}Au [3] and ^{185}Hg [5] in the heavy-ion-induced fusion-evaporation reactions. It is natural to expect that an oblate two-quasiparticle band based on the $\pi h^{-1}_{11/2} \otimes \nu i^{-1}_{13/2}$ configuration might be observed in ^{184}Au, which would extend our knowledge of shape coexistence in the odd-odd Au isotopes.

One prominent feature of rotational spectra in the transitional Ir-Pt-Au region is the low-frequency $\pi h_{9/2}$ crossing. Usually, the origin of the first band crossings in the well-deformed rare-earth nuclei has been attributed to the alignment of a pair of $i_{13/2}$ neutrons. However, in the Ir-Pt-Au region, the Fermi surface enters the proton $h_{9/2}$ subshell and the $(\pi h_{9/2})^2$ alignment is getting competitive. Hence the first band crossing becomes far less clear in this mass region. For instance, the observed first band crossing in the $\nu i_{13/2}$ band of ^{185}Pt has been attributed to the $(\pi h_{9/2})^2$ alignment [7,8], whereas it has been interpreted as the $(\nu i_{13/2})^2$ alignment in the case of ^{183}Pt [4]. Based on the blocking arguments and quasiparticle alignment properties, the low-frequency $\pi h_{9/2}$ crossing has been proposed in Ir, Pt, and Au isotopes [2,3,7–15]. It is known that blocking arguments in odd-mass nuclei are somewhat ambiguous since one does not have control of the other type of nucleon. However, the band structures in an odd-odd nucleus may give us the chance to have different crossings blocked such that we can better understand the nature of those crossings in the neighboring nuclei.

Another remarkable nature of the band structures in doubly odd nuclei is the well-known low-spin signature inversion [16]. For a two-quasiparticle configuration in an odd-odd nucleus, the favored signature is defined as $\alpha_f = 1/2 \times (-1)^{j_\pi - 1/2} + 1/2 \times (-1)^{j_\nu - 1/2}$, while the unfavored signature is determined by $\alpha_{uf} = 1/2 \times (-1)^{j_\pi - 1/2} + 1/2 \times (-1)^{j_\nu + 1/2}$ or $\alpha_{uf} = 1/2 \times (-1)^{j_\pi + 1/2} + 1/2 \times (-1)^{j_\nu - 1/2}$, where j_π and j_ν are the angular momenta of the valence proton and neutron, respectively. Generally, the levels with α_f are expected to lie lower in energy than the levels with α_{uf}. However, this rule is broken in a number of bands with certain configurations; that is, the favored signature branch lies higher in energy than the unfavored signature at low spins. This is the so-called low-spin signature inversion [16], which has been systematically observed in deformed odd-odd nuclei throughout the chart of nuclides in the $\pi g_{9/2} \otimes \nu g_{9/2}$ ($A \sim 80$), $\pi h_{11/2} \otimes \nu h_{11/2}$ ($A \sim 130$), $\pi h_{11/2} \otimes \nu i_{13/2}$ ($A \sim 160$), $\pi h_{9/2} \otimes \nu i_{13/2}$ ($A \sim 170$), and $\pi i_{13/2} \otimes \nu i_{13/2}$ ($A \sim 180$) configurations (see Refs. [17–19] and references therein). Such an anomalous phenomenon has been attracting large experimental and theoretical interests. From systematic analyses for the bands of the $\pi h_{9/2} \otimes \nu i_{13/2}$ configuration, one has found a common feature that the two signature branches cross each other at a certain high-spin value, beyond which normal signature

*yhzhang@impcas.ac.cn

splitting would be observed. This crossing phenomenon can be regarded as indirect evidence of low-spin signature inversion. In ^{184}Au, both the $\pi h_{9/2} \otimes \nu i_{13/2}$ and $\pi i_{13/2} \otimes \nu i_{13/2}$ bands have been observed by Ibrahim *et al.* [6]. The $\pi h_{9/2} \otimes \nu i_{13/2}$ band shows apparent signature splitting at low-spin states and the two signature branches tend to cross each other. If the original level spins [6] were accepted, the low-spin signature inversion would not be observed, which is contrary to the systematic studies [19,20]. Therefore one may need to reevaluate the level spins. For the $\pi i_{13/2} \otimes \nu i_{13/2}$ band, both signature splitting and crossing tendency have been observed, although no spin assignment was made [6]. If one extends the $\pi h_{9/2} \otimes \nu i_{13/2}$ and $\pi i_{13/2} \otimes \nu i_{13/2}$ bands of ^{184}Au to higher spin states, the signature crossing phenomenon might be observed in both bands, which would help to clarify the level spins for the two structures.

Based on the considerations mentioned above, the doubly odd nucleus ^{184}Au with $Z = 79$ and $N = 105$ seems to be a good candidate for studies on shape coexistence, band crossing, and low-spin signature inversion. Prior to this work, low-spin states of ^{184}Au were studied using the β^+/EC decay of ^{184}Hg [21], and four rotational bands were established by means of in-beam γ-ray spectroscopic techniques [6]. In order to get more information about the band structures of ^{184}Au, further investigations have been carried out by using in-beam γ-spectroscopy techniques. When this work was in progress, Sauvage *et al.* [22] reported a further study on low-spin states of ^{184}Au, which could help us to obtain a better understanding of the features of high-spin states in ^{184}Au. In this article, we report the experimental results on high-spin structures in ^{184}Au. Preliminary reports of this work have been published elsewhere [23–26]. The more detailed results are presented in this paper.

II. EXPERIMENTAL DETAILS AND RESULTS

A. Measurements

High-spin states in ^{184}Au were populated via the ^{159}Tb(^{29}Si, $4n\gamma$) reaction at a bombarding energy of 140 MeV. The ^{29}Si beam of 8 pnA was provided by the accelerator complex of the Tandem-XTU and ALPI at the Laboratori Nazionali di Legnaro, Italy. The target consisted of an enriched ^{159}Tb metallic foil of 2 mg/cm^2 thickness backed with a 5 mg/cm^2 evaporated Au layer. In-beam γ rays were detected by the GASP multidetector array, which consists of 40 Compton-suppressed large-volume Ge detectors and a multiplicity filter of 80 BGO elements. The energy and efficiency calibrations were made using ^{56}Co, ^{133}Ba, and ^{152}Eu standard sources. Events were collected when at least three suppressed Ge and two inner multiplicity filter detectors were fired. This triggering condition has proven to be very important and essential for suppressing the contaminated γ rays of low multiplicity from fission products and long-lived residues. A total of 2.0×10^8 events were recorded. After accurate gain matching, these coincidence events were sorted into fully symmetrized E_γ-E_γ matrices and E_γ-E_γ-E_γ cubes for subsequent off-line analysis. In this experiment, the most intensely populated nuclei were ^{183,184,185}Au [2,3,27], ^{183,184}Pt [4,11], and ^{181}Ir [28], corresponding to $5n$, $4n$, $3n$, $4np$, $3np$, and $\alpha 3n$ evaporation channels, respectively. In order to search for the new bands belonging to ^{184}Au, the sum energy and multiplicity of the γ rays detected by the BGO multiplicity filter were also recorded. In the off-line analysis, an asymmetric matrix of γ-ray energy in the Ge detectors versus sum energy in the BGO multiplicity filter was used to find assignments of γ transitions to different reaction products.

A method based on the observation of directional correlations of γ rays deexciting oriented states (DCO ratios) was adopted to determine the multipolarities of γ-ray transitions and the relative spins of the nuclear levels. For this purpose, the coincidence data were sorted into an asymmetric matrix with one γ ray detected in one of 12 detectors placed at 31.7°, 36°, 144°, and 148.3° (with the average angles being 34° and 146°) and the other one detected in one of the 8 detectors at 90° with respect to the beam direction. The γ-ray intensities $I_\gamma(34^\circ)$ and $I_\gamma(90^\circ)$, used to determine the DCO ratios defined as $R_{\rm DCO}(\gamma) = I_\gamma(34^\circ)/I_\gamma(90^\circ)$, were extracted from the coincidence spectra by setting gates on the 90° and 34° axes, respectively, of the above-mentioned asymmetric matrix. In the GASP geometry, by setting gates on stretched quadrupole transitions, $R_{\rm DCO}(\gamma)$ values were close to unity for stretched quadrupole transitions and $\sim$0.5 for dipole ones.

B. Level scheme

The previous low-spin and high-spin studies on ^{184}Au [6,21] provide an important basis for the present work. Most of the γ rays reported in the literature [6] were observed in this experiment. Assignments of the newly observed γ rays to ^{184}Au were based on the coincidences with the known γ rays [6,21]. The sum energy of the γ rays detected by the BGO multiplicity filter, combined with Au K x rays coincident information, gave us additional information to assign new γ-ray cascades to ^{184}Au. Gated spectra were produced for each of the γ rays assigned to ^{184}Au. From detailed analyses of the coincidence data, a level scheme of ^{184}Au consisting of seven rotational bands and an irregular structure has been established and is presented in Fig. 1 with bands labeled numerically. The ordering of transitions in the level scheme was determined according to the γ-γ coincidence relationships, γ-ray relative intensities, and γ-ray energy sums. The spins and parities for the known levels were partially adopted from the previous works [6,21,29], and these values were used as the references of the spin and parity assignments for the newly observed states. In the present work, we have used the general yrast argument that levels populated in heavy-ion-induced fusion-evaporation reactions usually have spins increasing with increasing excitation energy. Therefore, the measured DCO ratios allow straightforward determinations of spins and parities for the excited states in ^{184}Au. In addition, systematic comparisons with neighboring nuclei and arguments based on band configurations have also been used for the spin and parity assignments.

In the present study, the level scheme of ^{184}Au has been significantly extended in comparison with the previous result [6]. In Fig. 1, bands 1–4 were reported by Ibrahim *et al.* [6].

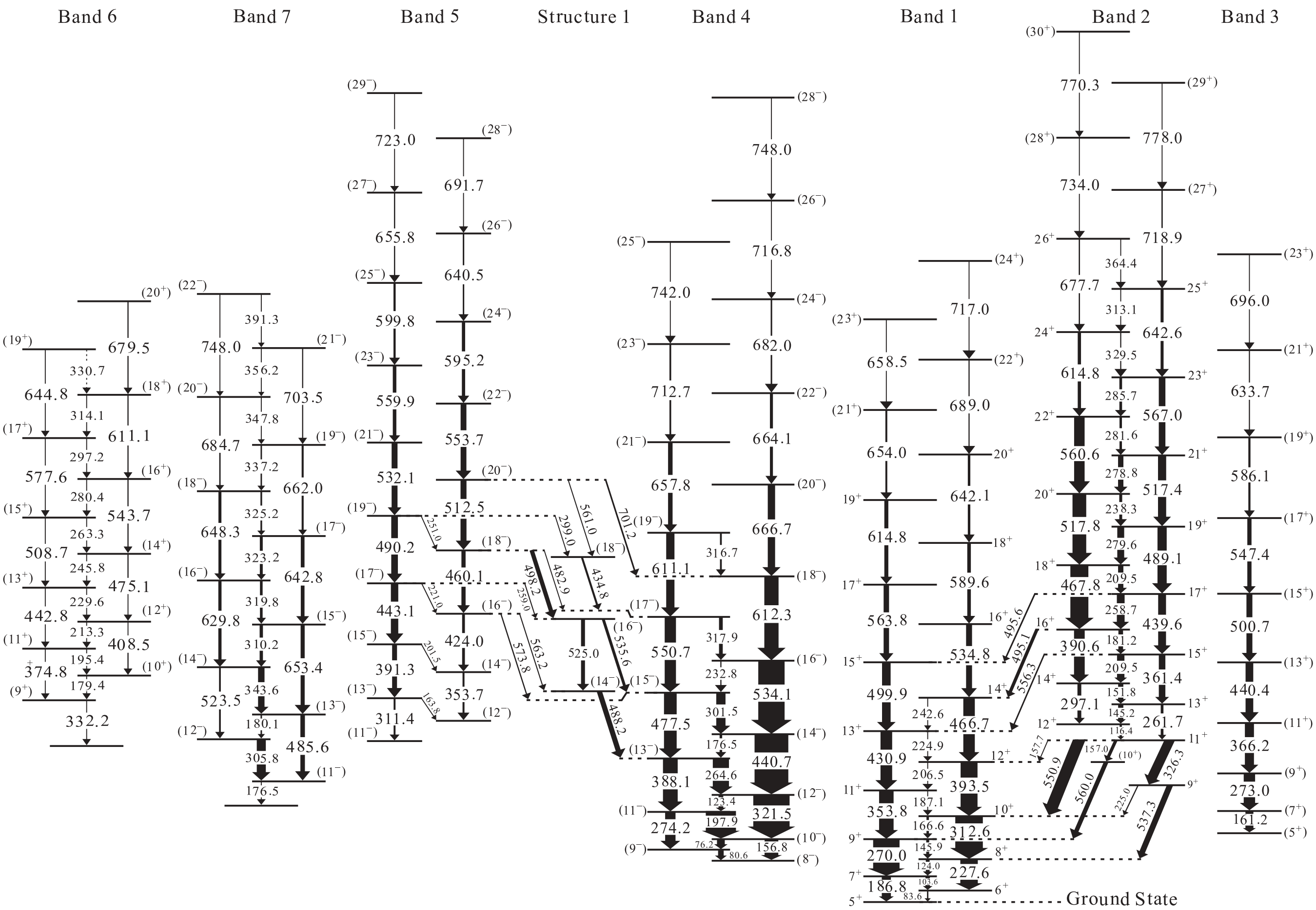

FIG. 1. Level scheme of ^{184}Au deduced from the present work.

These four bands have been extended to higher spins and for the cases of bands 1, 2, and 4 also to lower spins. Three new bands (labeled as bands 5–7) have been identified. For bands 1 and 3, the spin and parity assignments of Ref. [6] have been adopted. In the remainder of this section, a detailed description of the level scheme will be presented and explained. Typical coincidence spectra are shown in Figs. 2–7, where the γ transitions are indicated by the γ-ray energies (in keV).

The ground-state spin and parity of ^{184}Au were determined to be $I^\pi = 5^+$ from the study of ^{184}Hg β^+/EC decay [21], which was further confirmed by a resonance ionization spectroscopy experiment [29]. Ibrahim and co-workers have established the ground-state band [6], corresponding to band 1 in Fig. 1. However, the ground-state band was not connected to the 5^+ ground state and the lowest level of this band was assigned to be the (6^+) state [6]. In our previous report [23], two γ rays with energies of 83.6 and 186.8 keV were assigned to connect the (6^+) and (7^+) states in the ground-state band [6] with the 5^+ ground state, respectively. Consequently, a definitive spin assignment for band 1 was obtained [23]. In this paper, the coincidence spectra of Fig. 2 are presented to emphasize the two γ rays. The deduced DCO ratios for the 83.6- and 186.8-keV transitions [$R_{\rm DCO}(83.6\ {\rm keV}) = 0.51(14)$ and $R_{\rm DCO}(186.8\ {\rm keV}) = 1.08(14)$] indicate they are $M1/E2$ and $E2$ transitions, respectively, which is in agreement with the spin assignment for band 1. In addition, band 1 has been extended from $I^\pi = 17^+$ up to $I^\pi = (24^+)$. Some newly observed γ lines can be clearly seen in Fig. 2.

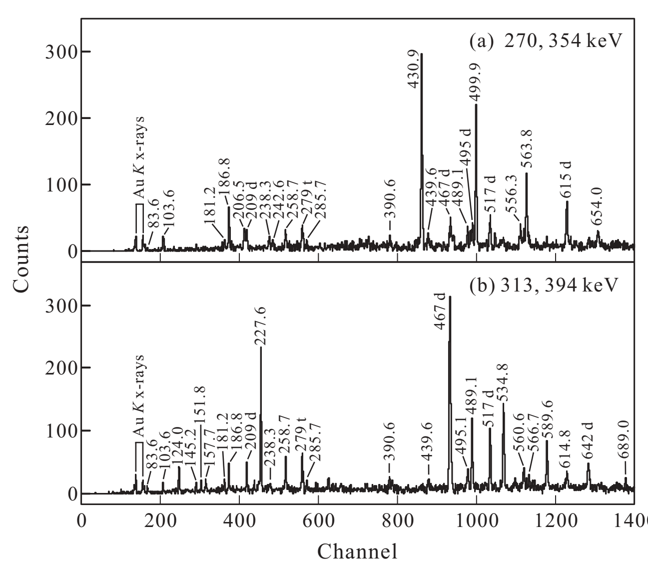

FIG. 2. Coincidence spectra double gated on transitions of (a) the $\alpha = 1$ sequence of band 1 (270 and 354 keV) and (b) the $\alpha = 0$ sequence of band 1 (313 and 394 keV). The lines with d and t correspond to doublet and triplet γ transitions, respectively.

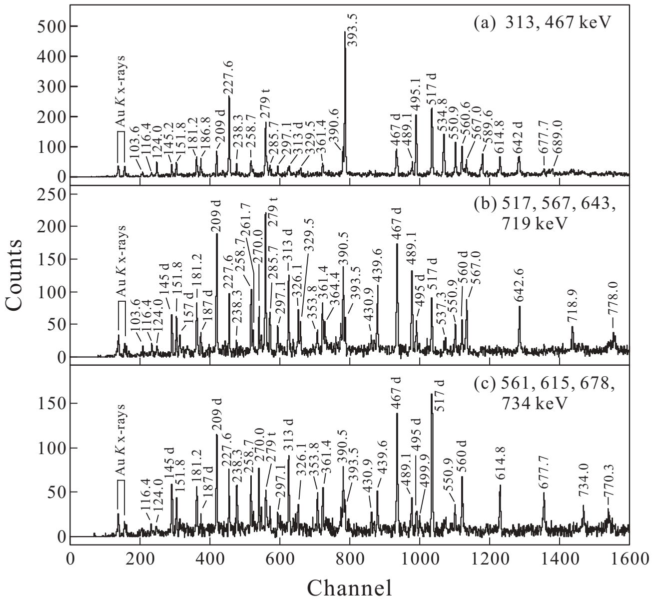

FIG. 3. (a) Coincidence spectrum double gated on the 313- and 467-keV γ rays. (b) Summed spectrum double gated on the 517-, 567-, 643-, and 719-keV γ rays in the $\alpha = 1$ sequence of band 2. (c) Summed spectrum double gated on the 561-, 615-, 678-, and 734-keV γ rays in the $\alpha = 0$ sequence of band 2.

Band 2 was assigned to be a positive-parity band in the work of Ibrahim *et al.* [6], but the level spins were not suggested. This band has also been discussed in our previous report [23]. Due to the observation of linking transitions between band 2 and band 1, the level spins of band 2 were fixed [23]. Figure 3(a) illustrates the existence of the 495.1- and 550.9-keV linking transitions by setting double gates on the 313- and 467-keV γ rays. With the help of the spin assignment for band 2 and the newly observed γ rays, band 2 has been extended from $I^\pi = 23^+$ up to $I^\pi = (30^+)$ and also from $I^\pi = 12^+$ down to $I^\pi = 11^+$. Coincidence spectra for the $\alpha = 1$ and $\alpha = 0$ sequences are presented in Figs. 3(b) and 3(c), respectively.

All the reported γ transitions in band 3 [6] were observed in this experiment and their quadrupole character was confirmed in the present work. In addition, a cascade of γ rays of 568.1-, 633.7-, and 696.0-keV transitions was added to the (17^+) state, extending this band up to the (23^+) state. As shown in Fig. 4, these new transitions can be clearly identified.

Band 4 was previously reported to be a negative-parity band [6]. We adopted the parity assignment for band 4, but the spins of levels were increased by one unit with respect to the original ones [6], which will be discussed in Sec. III E. In the lower part, the crossover transition of 274.2 (197.9 + 76.2) keV was observed, extending the $\alpha = 1$ sequence down to (9^-). From the coincidence spectrum double gated on the 157- and 321-keV γ rays, we found that the 157-keV line is a doublet. One of them should correspond to the 156.7-keV transition which deexcites the 3^-, 69 ± 6 ns isomer [21]. The second 157-keV transition might be a member of band 4. With the observation of the 80.6-keV line, we assigned the second 157-keV transition as the 156.8 (80.6 + 76.2) keV,

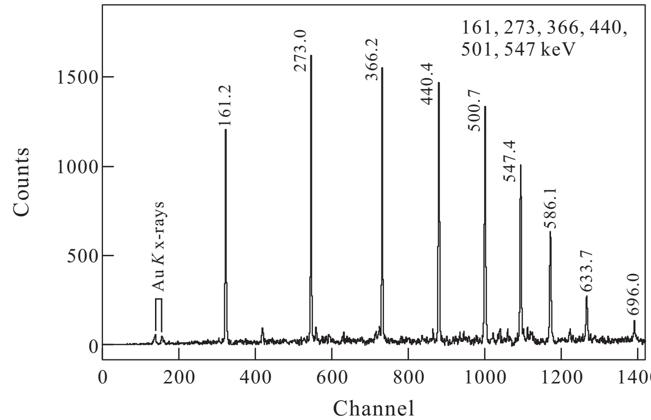

FIG. 4. Summed spectrum double gated on the 161-, 273-, 366-, 440-, 501-, and 547-keV γ rays in band 3.

$(10^-) \to (8^-)$ crossover transition in the $\alpha = 0$ sequence of band 4. In addition, the 156.8-keV transition continues in the rotational-like behavior of the transition energies as a function of spin. In the upper part of band 4, four new transitions with energies of 611.1, 657.8, 712.7, and 742.0 keV were placed in the $\alpha = 1$ sequence and five new lines with energies of 666.7, 664.1, 682.0, 716.8 and 748.0 keV were assigned to the $\alpha = 0$ sequence, extending the two sequences up to (25^-) and (28^-) states, respectively. Representative double-gated spectra displaying the new transitions are shown in Fig. 5.

Structure 1 was established in this work. It consists of three levels, which depopulate into the (13^-), (15^-), and (17^-) levels of band 4 via transitions of 488.2, 535.6, and 434.8 keV, respectively. The deduced DCO ratios for the three transitions (see Table I) are all consistent with those of $\triangle I = 1, M1 + E2$ mixed transitions with negative $E2/M1$ mixing ratios. It is

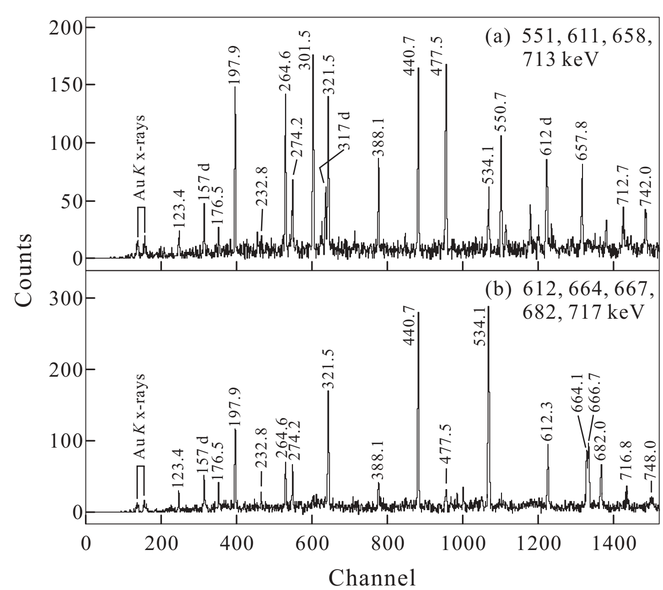

FIG. 5. (a) Summed spectrum double gated on the 551-, 611-, 658-, and 713-keV γ rays in the $\alpha = 1$ sequence of band 4. (b) Summed spectrum double gated on the 612-, 664-, 667-, 682-, and 717-keV γ rays in the $\alpha = 0$ sequence of band 4.

TABLE I. γ-ray transition energies, spin and parity assignments, relative intensities, branching ratios, extracted $B(M1)/B(E2)$ ratios, and DCO ratios in ^{184}Au.

E_γ (keV)[a]	$J_i^\pi \to J_f^\pi$[b]	I_γ[c]	λ[d]	$B(M1)/B(E2)$[e]	R_{DCO}
Band 1					
83.6	$6^+ \to 5^+$	⩾50			0.51(14)
186.8	$7^+ \to 5^+$	331			1.08(14)
103.6	$7^+ \to 6^+$	160	2.07(15)	0.069(5)	0.62(21)
227.6	$8^+ \to 6^+$	634			1.03(6)
124.0	$8^+ \to 7^+$	137	4.63(29)	0.048(3)	0.40(4)
270.0	$9^+ \to 7^+$	957			1.02(7)
145.9	$9^+ \to 8^+$	107	8.90(70)	0.036(3)	0.39(6)
312.6	$10^+ \to 8^+$	1000			0.98(6)
166.6	$10^+ \to 9^+$	88	11.32(67)	0.040(2)	0.31(5)
353.8	$11^+ \to 9^+$	526			1.10(8)
187.1	$11^+ \to 10^+$	23			
393.5	$12^+ \to 10^+$	613			1.05(7)
206.5	$12^+ \to 11^+$	24	25.06(2.29)	0.030(3)	0.27(7)
430.9	$13^+ \to 11^+$	423			1.02(7)
224.9	$13^+ \to 12^+$	17	24.21(2.33)	0.038(3)	
466.7	$14^+ \to 12^+$	417			1.09(10)
242.6	$14^+ \to 13^+$	16			
499.9	$15^+ \to 13^+$	311			1.02(8)
534.8	$16^+ \to 14^+$	216			1.02(11)
563.8	$17^+ \to 15^+$	197			0.97(11)
589.6	$18^+ \to 16^+$	130			1.06(17)
614.8	$19^+ \to 17^+$	145			1.19(25)
642.1	$20^+ \to 18^+$	91			1.08(17)
654.0	$(21^+) \to 19^+$	69			0.91(23)
689.0	$(22^+) \to 20^+$	41			0.93(24)
658.5	$(23^+) \to (21^+)$	21			
717.0	$(24^+) \to (22^+)$				
Band 2					
116.4	$12^+ \to 11^+$	85			0.58(9)
261.7	$13^+ \to 11^+$	99			1.13(17)
145.2	$13^+ \to 12^+$	189	0.31(2)	0.90(6)	0.59(7)
297.1	$14^+ \to 12^+$	140			0.90(11)
151.8	$14^+ \to 13^+$	189	0.52(3)	0.90(5)	0.56(7)
361.4	$15^+ \to 13^+$	238			1.01(8)
209.5	$15^+ \to 14^+$	269	0.90(5)	0.69(7)	0.51(5)
390.6	$16^+ \to 14^+$	388			1.00(7)
181.2	$16^+ \to 15^+$	169	1.56(9)	0.68(4)	0.50(5)
439.6	$17^+ \to 15^+$	285			1.04(9)
258.7	$17^+ \to 16^+$	282	1.07(6)	0.62(3)	0.37(4)
467.8	$18^+ \to 16^+$	653			0.97(8)
209.5	$18^+ \to 17^+$	192	2.46(37)	0.69(10)	0.42(6)
489.1	$19^+ \to 17^+$	334			1.02(9)
279.6	$19^+ \to 18^+$	251	1.16(16)	0.77(11)	
517.8	$20^+ \to 18^+$	498			0.99(8)
238.3	$20^+ \to 19^+$	107	3.45(47)	0.56(8)	0.43(6)
517.4	$21^+ \to 19^+$	296			1.02(13)
278.8	$21^+ \to 20^+$	194			0.68(7)
560.6	$22^+ \to 20^+$	381			1.06(10)
281.6	$22^+ \to 21^+$	89	3.00(26)	0.58(5)	0.45(3)
567.0	$23^+ \to 21^+$	240			1.14(13)
285.7	$23^+ \to 22^+$	98	2.44(17)	0.72(5)	0.47(3)
614.8	$24^+ \to 22^+$	119			1.02(18)
329.5	$24^+ \to 23^+$	40	2.94(29)	0.58(6)	0.43(6)
642.6	$25^+ \to 23^+$	108			1.13(17)
313.1	$25^+ \to 24^+$				

TABLE I. *(Continued.)*

E_γ (keV)[a]	$J_i^\pi \rightarrow J_f^\pi$[b]	I_γ[c]	λ[d]	$B(M1)/B(E2)$[e]	R_{DCO}
677.7	$26^+ \rightarrow 24^+$	46			1.19(24)
364.4	$26^+ \rightarrow 25^+$	22	3.19(47)	0.64(10)	0.59(08)
718.9	$(27^+) \rightarrow 25^+$	48			
734.0	$(28^+) \rightarrow 26^+$	30			
778.0	$(29^+) \rightarrow (27^+)$				
770.3	$(30^+) \rightarrow (28^+)$				
Band 3					
161.2	$(7^+) \rightarrow (5^+)$	288			1.10(11)
273.0	$(9^+) \rightarrow (7^+)$	413			0.95(7)
366.2	$(11^+) \rightarrow (9^+)$	329			1.09(8)
440.4	$(13^+) \rightarrow (11^+)$	279			1.01(8)
500.7	$(15^+) \rightarrow (13^+)$	215			0.97(9)
547.4	$(17^+) \rightarrow (15^+)$	152			0.86(8)
586.1	$(19^+) \rightarrow (17^+)$	77			1.00(21)
633.7	$(21^+) \rightarrow (19^+)$	40			
696.0	$(23^+) \rightarrow (21^+)$	11			
Band 4					
80.6	$(9^-) \rightarrow (8^-)$	$\geqslant$204			
156.8	$(10^-) \rightarrow (8^-)$	$<$497			
76.2	$(10^-) \rightarrow (9^-)$	283			
274.2	$(11^-) \rightarrow (9^-)$	377			1.07(16)
197.9	$(11^-) \rightarrow (10^-)$	1094	0.35(3)	0.40(3)	0.28(3)
321.5	$(12^-) \rightarrow (10^-)$	1317			0.97(7)
123.4	$(12^-) \rightarrow (11^-)$	171	7.70(94)	0.16(2)	0.63(10)
388.1	$(13^-) \rightarrow (11^-)$	534			1.04(16)
264.6	$(13^-) \rightarrow (12^-)$	586	0.91(12)	0.36(5)	0.39(3)
440.7	$(14^-) \rightarrow (12^-)$	1224			0.98(6)
176.5	$(14^-) \rightarrow (13^-)$	93	13.19(82)	0.16(1)	0.49(7)
477.5	$(15^-) \rightarrow (13^-)$	460			0.98(15)
301.5	$(15^-) \rightarrow (14^-)$	335	1.37(14)	0.46(5)	0.34(3)
534.1	$(16^-) \rightarrow (14^-)$	955			1.14(12)
232.8	$(16^-) \rightarrow (15^-)$	42	22.78(1.93)	0.10(1)	0.61(14)
550.7	$(17^-) \rightarrow (15^-)$	409			1.12(13)
317.9	$(17^-) \rightarrow (16^-)$	136	3.01(19)	0.36(2)	0.36(3)
612.3	$(18^-) \rightarrow (16^-)$	516			0.99(5)
611.1	$(19^-) \rightarrow (17^-)$	300			1.04(15)
316.7	$(19^-) \rightarrow (18^-)$	67			0.35(9)
666.7	$(20^-) \rightarrow (18^-)$	266			0.97(14)
657.8	$(21^-) \rightarrow (19^-)$	164			1.03(11)
664.1	$(22^-) \rightarrow (20^-)$	109			1.04(20)
712.7	$(23^-) \rightarrow (21^-)$	63			0.97(13)
682.0	$(24^-) \rightarrow (22^-)$	55			
742.0	$(25^-) \rightarrow (23^-)$				
716.8	$(26^-) \rightarrow (24^-)$	24			
748.0	$(28^-) \rightarrow (26^-)$				
Band 5					
311.4	$(13^-) \rightarrow (11^-)$	$\geqslant$69			1.01(13)
163.8	$(13^-) \rightarrow (12^-)$	$\geqslant$14	3.50(59)	0.13(2)	0.60(7)
353.7	$(14^-) \rightarrow (12^-)$	$\geqslant$71			1.09(19)
391.3	$(15^-) \rightarrow (13^-)$	$\geqslant$178			0.89(9)
201.5	$(15^-) \rightarrow (14^-)$	$\geqslant$34	5.29(35)	0.16(3)	0.45(8)
424.0	$(16^-) \rightarrow (14^-)$	101			1.25(23)
443.1	$(17^-) \rightarrow (15^-)$	268			1.04(9)
221.0	$(17^-) \rightarrow (16^-)$	35	7.76(77)	0.14(1)	0.58(13)
460.1	$(18^-) \rightarrow (16^-)$	151			1.16(22)
490.2	$(19^-) \rightarrow (17^-)$	241			1.03(9)

TABLE I. *(Continued.)*

E_γ (keV)[a]	$J_i^\pi \rightarrow J_f^\pi$[b]	I_γ[c]	λ[d]	$B(M1)/B(E2)$[e]	R_{DCO}
251.0	$(19^-) \rightarrow (18^-)$	17	14.11(1.25)	0.09(1)	0.47(7)
512.5	$(20^-) \rightarrow (18^-)$	216			0.96(11)
532.1	$(21^-) \rightarrow (19^-)$	214			0.98(11)
553.7	$(22^-) \rightarrow (20^-)$	210			1.05(17)
559.9	$(23^-) \rightarrow (21^-)$	129			0.94(10)
595.2	$(24^-) \rightarrow (22^-)$	119			0.82(14)
599.8	$(25^-) \rightarrow (23^-)$	79			1.06(15)
640.5	$(26^-) \rightarrow (24^-)$	54			1.03(26)
655.8	$(27^-) \rightarrow (25^-)$	44			
691.7	$(28^-) \rightarrow (26^-)$				
723.0	$(29^-) \rightarrow (27^-)$	21			
Band 6					
332.2[f]	$(9^+) \rightarrow$				
179.4	$(10^+) \rightarrow (9^+)$				
374.8	$(11^+) \rightarrow (9^+)$				
195.4	$(11^+) \rightarrow (10^+)$		0.19(4)	3.64(77)	
408.5	$(12^+) \rightarrow (10^+)$				
213.3	$(12^+) \rightarrow (11^+)$		0.33(5)	2.48(38)	
442.8	$(13^+) \rightarrow (11^+)$				
229.6	$(13^+) \rightarrow (12^+)$		0.40(7)	2.45(43)	
475.1	$(14^+) \rightarrow (12^+)$				
245.8	$(14^+) \rightarrow (13^+)$		0.59(9)	1.93(29)	
508.7	$(15^+) \rightarrow (13^+)$				
263.3	$(15^+) \rightarrow (14^+)$		1.11(29)	1.17(31)	
543.7	$(16^+) \rightarrow (14^+)$				
280.4	$(16^+) \rightarrow (15^+)$				
577.6	$(17^+) \rightarrow (15^+)$				
297.2	$(17^+) \rightarrow (16^+)$				
611.1	$(18^+) \rightarrow (16^+)$				
314.1	$(18^+) \rightarrow (17^+)$				
644.8	$(19^+) \rightarrow (17^+)$				
330.7	$(19^+) \rightarrow (18^+)$				
679.5	$(20^+) \rightarrow (18^+)$				
Band 7					
176.5[f]	$(11^-) \rightarrow$	$\geqslant 29$			
305.8	$(12^-) \rightarrow (11^-)$	328			0.65(11)
485.6	$(13^-) \rightarrow (11^-)$	164			1.05(18)
180.1	$(13^-) \rightarrow (12^-)$	53	3.10(21)	1.04(7)	0.63(12)
523.5	$(14^-) \rightarrow (12^-)$	64			
343.6	$(14^-) \rightarrow (13^-)$	234	0.27(4)	2.50(37)	0.65(9)
653.4	$(15^-) \rightarrow (13^-)$	147			1.10(13)
310.2	$(15^-) \rightarrow (14^-)$	120	1.23(9)	2.26(16)	0.62(11)
629.8	$(16^-) \rightarrow (14^-)$	116			1.16(21)
319.8	$(16^-) \rightarrow (15^-)$	97	1.19(10)	1.77(15)	0.61(11)
642.8	$(17^-) \rightarrow (15^-)$	135			1.17(24)
323.2	$(17^-) \rightarrow (16^-)$	106	1.31(34)	1.73(45)	0.56(10)
648.3	$(18^-) \rightarrow (16^-)$	108			1.09(11)
325.2	$(18^-) \rightarrow (17^-)$	61	1.76(22)	1.32(16)	0.62(17)
662.0	$(19^-) \rightarrow (17^-)$	73			1.03(27)
337.2	$(19^-) \rightarrow (18^-)$	52			
684.7	$(20^-) \rightarrow (18^-)$	50			
347.8	$(20^-) \rightarrow (19^-)$	17			
703.5	$(21^-) \rightarrow (19^-)$	41			
356.2	$(21^-) \rightarrow (20^-)$	19			
748.0	$(22^-) \rightarrow (20^-)$	25			
391.3	$(22^-) \rightarrow (21^-)$	15			

TABLE I. *(Continued.)*

E_γ (keV)[a]	$J_i^\pi \rightarrow J_f^\pi$[b]	I_γ[c]	λ[d]	$B(M1)/B(E2)$[e]	R_{DCO}
Structure 1					
525.0	$(16^-) \rightarrow (14^-)$	143			1.22(17)
Transitions	from band 2	to band 1			
157.7	$11^+ \rightarrow 12^+$	17			
495.1	$16^+ \rightarrow 14^+$	119			1.02(8)
495.6	$17^+ \rightarrow 15^+$	55			
550.9	$11^+ \rightarrow 10^+$	433			0.22(2)
556.3	$15^+ \rightarrow 13^+$	52			
Transitions	from band 5	to band 4			
482.9	$(18^-) \rightarrow (17^-)$	30			0.33(6)
573.8	$(16^-) \rightarrow (15^-)$	43			
701.2	$(20^-) \rightarrow (18^-)$	57			1.13(27)
Transitions	from band 5	to structure 1			
259.0	$(17^-) \rightarrow (16^-)$	37			0.61(15)
299.0	$(19^-) \rightarrow (18^-)$	28			0.46(7)
498.2	$(18^-) \rightarrow (16^-)$	154			1.22(18)
561.0	$(20^-) \rightarrow (18^-)$	35			
563.2	$(16^-) \rightarrow (14^-)$	37			
Transitions	from structure 1	to band 4			
434.8	$(18^-) \rightarrow (17^-)$	74			0.37(6)
488.2	$(14^-) \rightarrow (13^-)$	186			0.28(4)
535.6	$(16^-) \rightarrow (15^-)$	104			0.31(6)
Others					
157.0	$11^+ \rightarrow (10^+)$	117			
225.0	$9^+ \rightarrow 10^+$	42			0.58(7)
326.3	$11^+ \rightarrow 9^+$	350			1.18(13)
537.3	$9^+ \rightarrow 8^+$	207			0.43(5)
560.0	$(10^+) \rightarrow 9^+$	159			

[a]Uncertainties are within 0.5 keV.
[b]See text for details about the spin and parity assignments.
[c]Uncertainties are between 5% and 30%. Values are normalized to the 312.3-keV transition in band 1.
[d]Branching ratios $T_\gamma(I \rightarrow I-2)/T_\gamma(I \rightarrow I-1)$, $T_\gamma(I \rightarrow I-2)$, and $T_\gamma(I \rightarrow I-1)$ are the relative γ intensities of the $E2$ and $M1$ transitions depopulating level I, respectively.
[e]Values are extracted from the branching ratios by assuming $\delta^2 = 0$.
[f]γ-ray deexciting the bandhead.

reasonable to assign the three γ lines as $(14^-) \rightarrow (13^-)$, $(16^-) \rightarrow (15^-)$, and $(18^-) \rightarrow (17^-)$ transitions, respectively.

Band 5 was newly observed in this experiment. It has two sequences of quadrupole transitions, which are connected by four weak in-band $\triangle I = 1$, $M1 + E2$ mixed transitions. Representative double-gated spectra on $E2$ transitions belonging to the $\alpha = 1$ and $\alpha = 0$ signature components of this band are shown in Figs. 6(a) and 6(b), respectively. As is clear in Fig. 6, the γ rays in band 5 are in coincidence with those γ lines in the low part of band 4. Based on the analyses of γ-γ coincidence relationships, three γ rays with energies of 482.9, 573.8, and 701.2 keV were observed to connect band 5 and band 4. Therefore, the level energies of band 5 relative to band 4 were unambiguously fixed, which is further confirmed by the observation of linking transitions between band 5 and structure 1. To determine the level spins and parities of band 5, the measured DCO ratios for the decay-out transitions of band 5 have been checked carefully. The DCO ratio for the most intense decay-out transition of 498.2 keV is 1.22(18), which indicates it is a stretched quadrupole transition. According to the general yrast argument, we assigned the level depopulated by the 498.2-keV transition as (18^-). Subsequently, the 701.2-keV line between band 5 and band 4 can be assigned as an $E2$, $(20^-) \rightarrow (18^-)$ transition, which is consistent with the measured DCO value [R_{DCO}(701.2 keV) = 1.13(27)].

Band 6 was identified in the present work and was weakly populated in the experiment. A summed double-gated spectrum demonstrating the existence of band 6 is shown in Fig. 7(a). One can see in Fig. 7(a) that the γ transitions in band 6 behave regularly. Since the 179.4-keV line is a relatively intensive γ transition in band 6 and it is the observed in-band $M1/E2$ transition with the lowest energy, it is reasonable to assume that the 179.4-keV line feeds the bandhead. Besides, the 332.2-keV line is strongly in coincidence with those transitions in band 6. We propose that the 332.2-keV line deexcites the bandhead. The γ rays in band 6 were found to be in coincidence with the Au K x rays, indicating that this band belongs to Au isotopes. Figure 8 presents the sum-energy spectra of the γ rays detected by

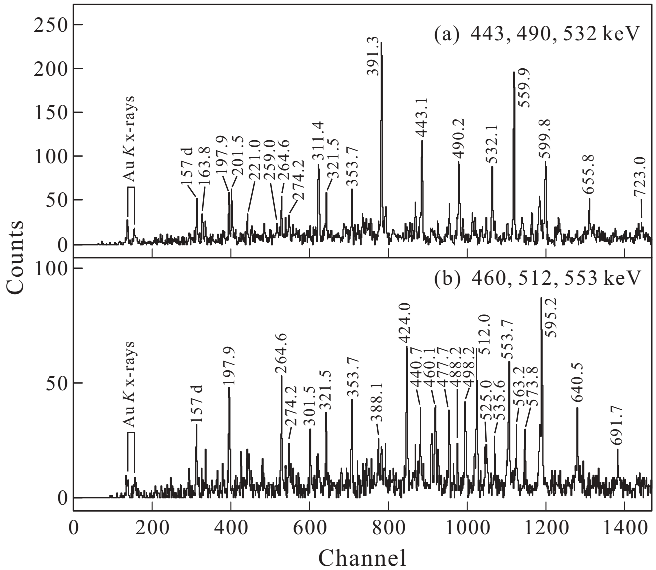

FIG. 6. (a) Summed spectrum double gated on the 443-, 490-, and 532-keV γ rays in the $\alpha = 1$ sequence of band 5. (b) Summed spectrum double gated on the 460-, 512-, and 553-keV γ rays in the $\alpha = 0$ sequence of band 5.

the BGO filter in coincidence with the 332-keV line and the known γ rays from ^{185}Au (287 keV) [3], ^{184}Au (354 keV) [6], and ^{183}Au (283 keV) [2]. It is shown that the average sum energies corresponding to the expected $3n$, $4n$, and $5n$ reaction channels can be well separated. The same average sum energies are clearly demonstrated in the figure for the 332- and 354-keV-gated spectra. In addition, the γ rays in band 6 were found to be in coincidence with the 156.7-keV line depopulating the 69 ± 6 ns isomer in ^{184}Au [21]. These experimental results support strongly the assignment of band 6

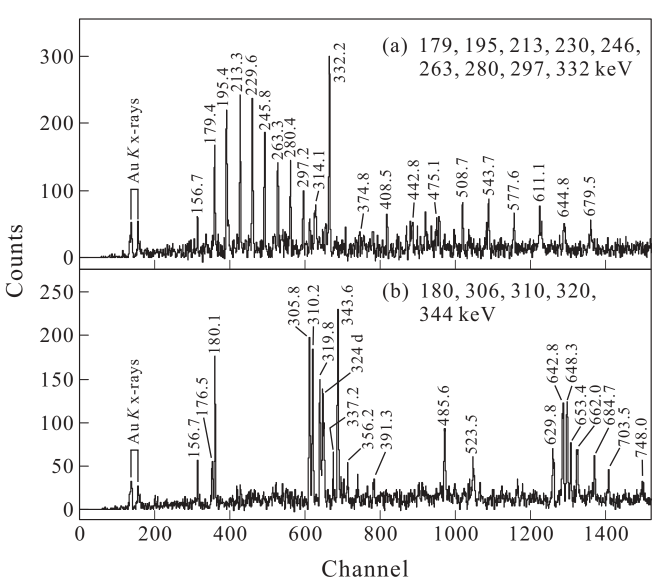

FIG. 7. (a) Summed spectrum double gated on the 179-, 195-, 213-, 230-, 246-, 263-, 280-, 297-, and 332-keV γ rays. (b) Summed spectrum double gated on the 180-, 306-, 310-, 320-, and 344-keV γ rays within band 7.

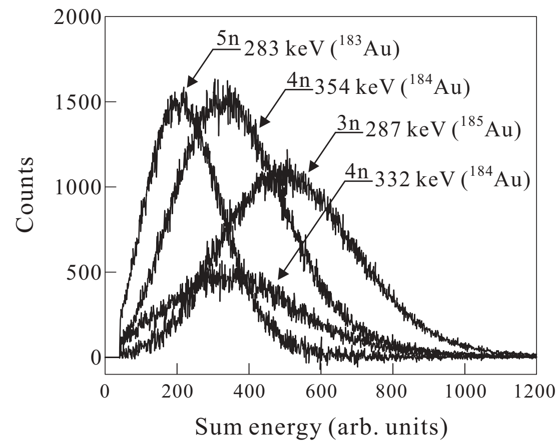

FIG. 8. Spectra of sum energy measured by the BGO filter in coincidence with γ rays from ^{183,184,185}Au.

to ^{184}Au. Following the same method used for the assignment of band 6, band 7 was assigned to ^{184}Au in our preliminary report [24]. A representative coincidence spectrum for band 7 is given in Fig. 7(b). Since both bands 6 and 7 are "floating" in energy, it is difficult to determine the spin and parity of the levels with a conventional spectroscopic method. Therefore the spin and parity assignments for the levels are completely based on theoretical assumptions and have tentative character.

C. Experimental transition probabilities

For the rotational bands shown in Fig. 1, the experimental branching ratios, which are defined as

$$\lambda = \frac{T_\gamma(I \to I-2)}{T_\gamma(I \to I-1)}, \quad (1)$$

were extracted for most of the transitions. Here $T_\gamma(I \to I-2)$ and $T_\gamma(I \to I-1)$ are the γ-ray intensities of the $\Delta I = 2$ and $\Delta I = 1$ transitions, respectively. The branching ratios were used to extract the experimental reduced transition probability ratios defined as

$$\frac{B(M1, I \to I-1)}{B(E2, I \to I-2)} = 0.697 \frac{E_\gamma(I \to I-2)}{E_\gamma(I \to I-1)} \frac{1}{\lambda} \frac{1}{1+\delta^2} \left(\frac{\mu_N^2}{e^2\,\mathrm{b}^2}\right), \quad (2)$$

where δ is the $E2/M1$ mixing ratio for the $\Delta I = 1$ transitions and $E_\gamma(I \to I-1)$ and $E_\gamma(I \to I-2)$ are the $\Delta I = 1$ and $\Delta I = 2$ transition energies (in MeV), respectively. In the calculation, δ has been set to zero, since no mixing ratio could be deduced from the present data; the error introduced under this assumption is expected to be less than 10%.

The relative intensities for some uncontaminated γ rays could be measured in the total projection spectrum. Most of the values were extracted from the gated spectra. The relative intensities are corrected with the detection efficiencies. For some weak or heavily contaminated γ rays, only upper or lower limits are given based on their intensity balances. The γ-ray energies, spin and parity assignments, relative γ-ray

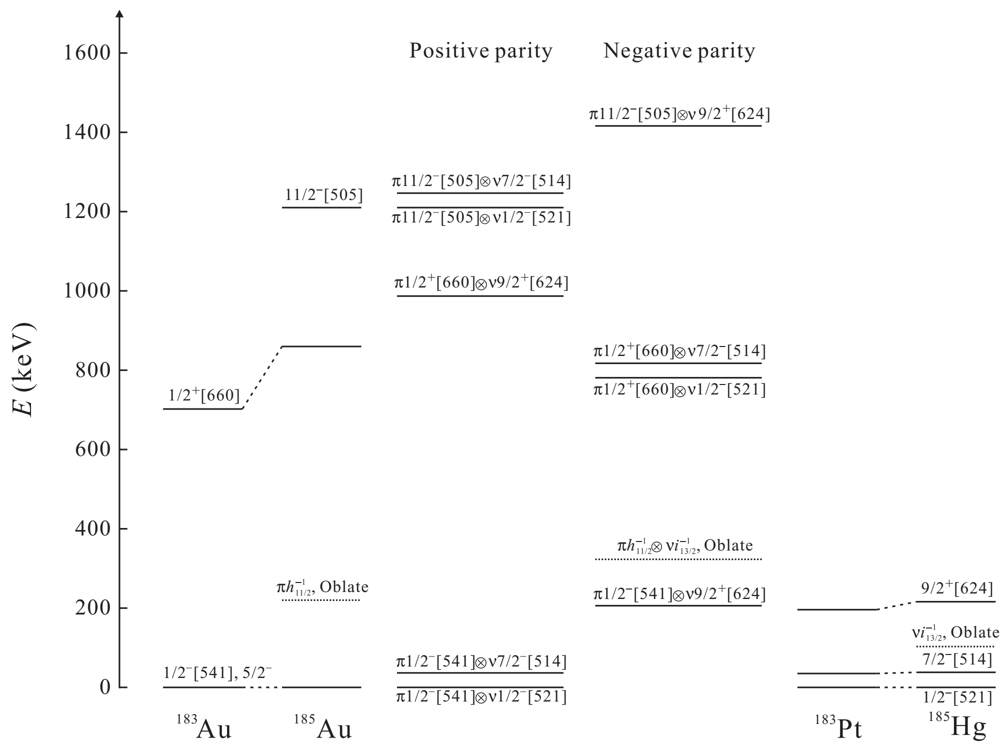

FIG. 9. Predicted bandhead excitation energies in ^{184}Au based on the zero-order approximation of Ref. [30].

intensities, branching rations, extracted $B(M1)/B(E2)$ values, and the DCO ratios are listed in Table I grouped in sequences for each band.

III. DISCUSSION

A. Preliminary remarks

The proton and neutron orbitals involved in the rotational bands of ^{184}Au can be identified on the basis of the coupling schemes proposed by Kreiner and co-workers [30]. The starting point is the construction of a zero-order level scheme, which would provide a qualitative idea of the relative energy location of different configurations. For the doubly odd nucleus ^{184}Au, the zero-order bandhead energies were obtained by adding the average experimental single-quasiparticle energies from neighboring odd nuclei, ^{183}Au [2,27], ^{185}Au [3], ^{183}Pt [4], and ^{185}Hg [5], and neglecting the residual interaction, which can split the $K_\pm = |\Omega_p \pm \Omega_n|$ states according to the Gallagher-Moszkowski coupling rules [31]. In this study, we have only taken the orbitals populated in the heavy-ion-induced fusion-evaporation reactions into account. Therefore, the prolate $\pi 11/2^-[505]$, oblate $\pi h^{-1}_{11/2}$, and oblate $\nu i^{-1}_{13/2}$ excitations were taken from ^{185}Au [3] and ^{185}Hg [5], respectively. Since the level spins have not been assigned for the $\pi 11/2^-[505]$ band in ^{185}Au [3], we have taken the excitation energy of the lowest level for calculations. The calculated results for the related two-quasiparticle intrinsic states in ^{184}Au are displayed in Fig. 9 and referenced in the following configuration assignments.

For a rotational band, the in-band transition properties are sensitive to the quasiparticle configurations; thus they are often used as criteria for configuration assignments. The theoretical estimates of the $B(M1)/B(E2)$ ratios were obtained from the semiclassical formula developed by Dönau and Frauendorf [32]. We used the following expressions:

$$B(M1, I \to I-1) = \frac{3}{8\pi}\mu_T^2 \tag{3}$$

and

$$B(E2, I \to I-2) = \frac{5}{16\pi}\langle IK20|I-2K\rangle^2 Q_0^2, \tag{4}$$

where μ_T is the transverse magnetic moment given by

$$\mu_T = \left(g_{\Omega_p} - g_R\right)\left(\Omega_p\sqrt{1-K^2/I^2} - i_p K/I\right) + \left(g_{\Omega_n} - g_R\right)\left(\Omega_n\sqrt{1-K^2/I^2} - i_n K/I\right), \tag{5}$$

in units of μ_N. Here Q_0 is the intrinsic quadrupole moment of the nucleus and g_{Ω_p} and g_{Ω_n} are the proton and neutron gyromagnetic factors, respectively. These values were taken from Refs. [29,33,34]. The quantities i_p and i_n represent the aligned angular momenta of the proton and the neutron, respectively. Alignments and g factors for the proton and neutron intrinsic states used in the calculations are listed in Table II. For the quadrupole moment, we referred to $Q_0 = 8.06e$ b, which corresponds to the value for the ground state of ^{184}Au [29]. A common collective gyromagnetic factor $g_R = 0.3$ was used in the calculations.

In the standard cranked shell model analysis [35], the quasiparticle alignment of a rotational band can be expressed as

$$i_x(\omega) = I_x(\omega) - R(\omega), \tag{6}$$

TABLE II. Parameters used in the calculations of $B(M1)$ values.

Protons			Neutrons		
Orbital	$i(\hbar)$	g_Ω	Orbital	$i(\hbar)$	g_Ω
$\pi 1/2^-[541]$	2.9[a]	0.84	$\nu 1/2^-[521]$	0.6[b]	0.79
$\pi 3/2^-[532]$	2.9[c]	0.61	$\nu 7/2^-[514]$	1.0[b]	0.25
$\pi 1/2^+[660]$	5.6[a]	1.35	$\nu 9/2^+[624]$	2.6[b]	−0.30
$\pi 11/2^-[505]$	1.0[d]	1.26			

[a]The value corresponds to ^{183}Au.
[b]The value corresponds to ^{183}Pt.
[c]The value is adopted from the $\pi 1/2^-[541]$ band of ^{183}Au.
[d]The value is estimated from the $\pi 11/2^-[505]$ band of ^{181}Au.

where $I_x(\omega)$ is the component of the total aligned angular momentum along the rotation axis and $R(\omega)$ is the collective contribution. The values of $I_x(\omega)$ and ω can be derived from the level spin I and the experimental level spacings,

$$I_x(\omega) = \sqrt{I(I+1) - K^2} \tag{7}$$

and

$$\hbar\omega = \frac{dE(I)}{dI_x(I)} \approx \frac{E(I+1) - E(I-1)}{I_x(I+1) - I_x(I-1)}. \tag{8}$$

The collective component is parametrized using the Harris expression

$$R(\omega) = J_0\omega + J_1\omega^3, \tag{9}$$

where the Harris parameters J_0 and J_1 can be extracted using the method proposed by Drissi and co-workers [36]. For prolate bands, a common reference with $J_0 = 24\hbar^2\ \mathrm{MeV}^{-1}$, $J_1 = 120\hbar^4\ \mathrm{MeV}^{-3}$ has been subtracted so that the unfavored signature branch of the $\pi h_{9/2} \otimes \nu i_{13/2}$ band in ^{184}Au has a constant alignment before the first band crossing. For oblate bands, we have chosen the parameters $J_0 = 8\hbar^2\ \mathrm{MeV}^{-1}$, $J_1 = 40\hbar^4\ \mathrm{MeV}^{-3}$, which have been frequently used in the neighboring nuclei [13,37]. The standard plots of the quasiparticle aligned angular i_x as a function of rotational frequency $\hbar\omega$ for prolate and oblate bands in ^{184}Au and neighboring nuclei are shown in Figs. 11 and 14, respectively.

B. Band 1

Band 1 is the ground-state band of ^{184}Au, which has been assigned as the $\pi h_{9/2} \otimes \nu 7/2^-[514]$ configuration [6]. In the neighboring ^{183,185}Au nuclei, the ground-state bands have been described by the $\pi h_{9/2}$-$1/2^-[541]$ configuration [2,3]. It is natural to expect that $\pi h_{9/2}$-$1/2^-[541]$ should be the main component in the ground-state band of ^{184}Au. However, resonance ionization spectroscopy performed by Le Blanc *et al.* [29] reveals that the 5^+ ground state has a pure value of $K = 5$, which means that the 5^+ ground state unambiguously corresponds to the configuration $\pi 3/2^-[532] \otimes \nu 7/2^-[514]$ with $K = \Omega_p + \Omega_n = 5$. The proton occupying the $\pi h_{9/2}$-$1/2^-[541]$ orbital in ^{183,185}Au [2,3] is in the $\pi h_{9/2}$-$3/2^-[532]$ orbital in ^{184}Au [29] for the ground states. Nevertheless, semimicroscopic model calculations performed by Sauvage *et al.* [22] suggest that the proton is predominately in the $\pi h_{9/2}$-$3/2^-[532]$ orbital for $I \leqslant 7$, whereas it is mainly in the $\pi h_{9/2}$-$1/2^-[541]$ orbital for $I > 7$ in the ground-state band of ^{184}Au. In Fig. 10(a), the measured experimental

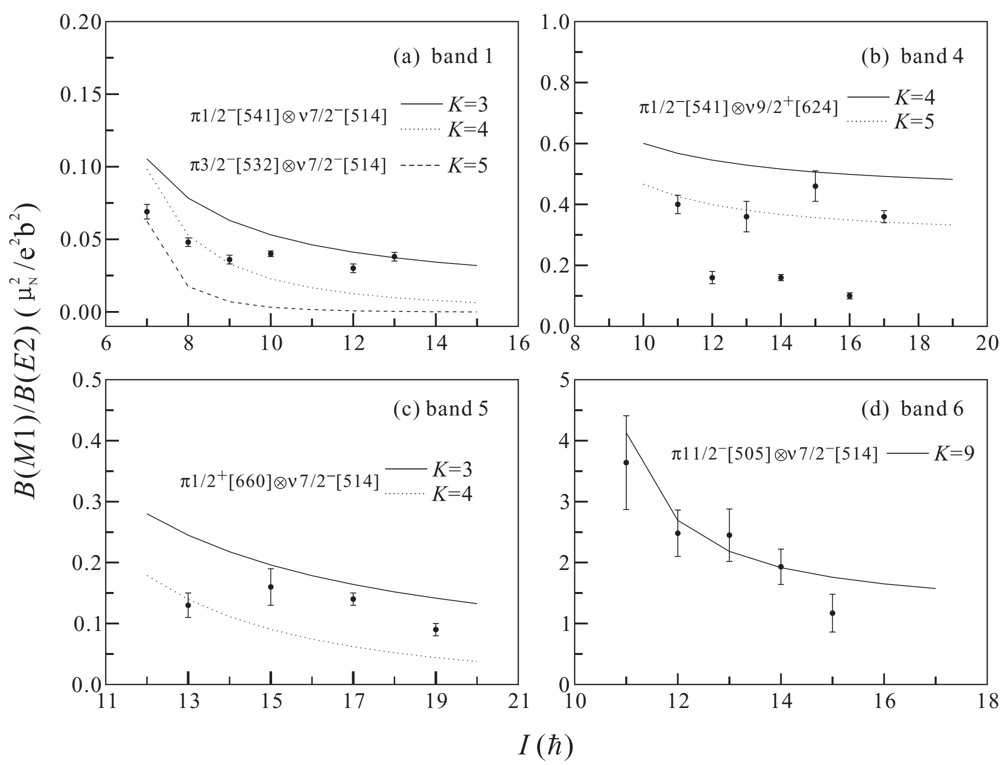

FIG. 10. Experimental and calculated $B(M1)/B(E2)$ values corresponding to (a) band 1, (b) band 4, (c) band 5, and (d) band 6.

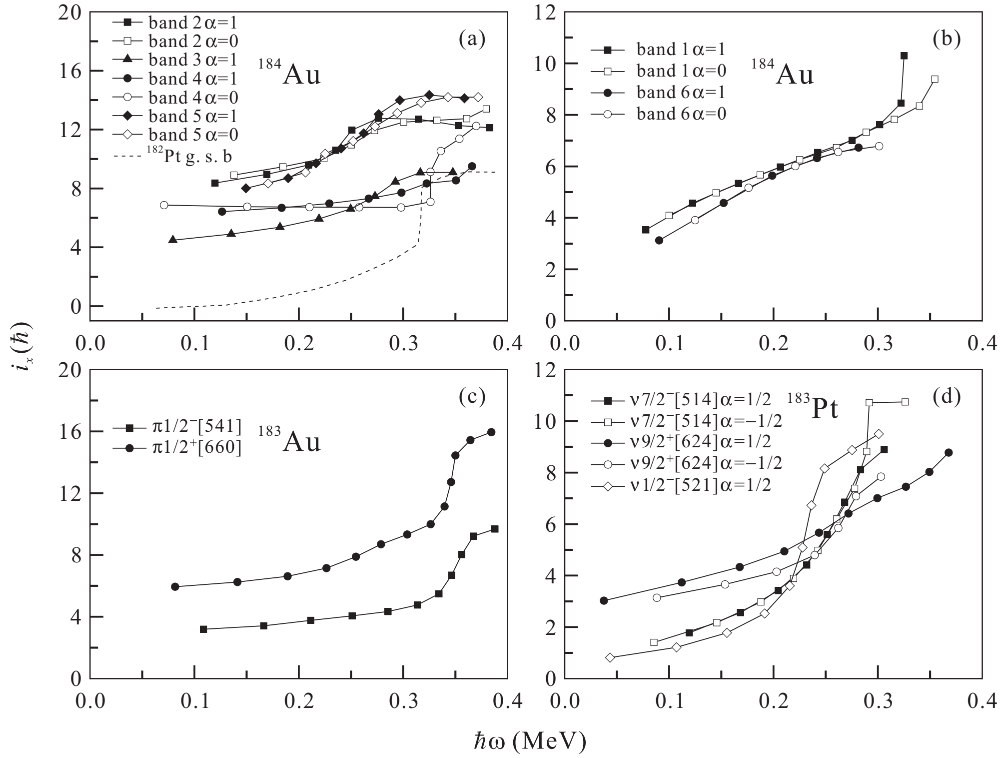

FIG. 11. Aligned angular momenta i_x as a function of rotational frequency for prolate bands in ^{184}Au and neighboring nuclei. The rotating reference is described by the parameters $J_0 = 24\hbar^2$ MeV^{-1}, $J_1 = 120\hbar^4$ MeV^{-3}.

$B(M1)/B(E2)$ ratios are compared with the theoretical predictions for the $\pi 3/2^-[532] \otimes \nu 7/2^-[514]$ and $\pi 1/2^-[541] \otimes \nu 7/2^-[514]$ configurations, respectively. As is illustrated in Fig. 10(a), the experimental $B(M1)/B(E2)$ ratio at spin $I = 7$ can be well reproduced by the configuration of $\pi 3/2^-[532] \otimes \nu 7/2^-[514]$. For spins $I \geqslant 8$, the experimental values are in fair agreement with the calculated ones associated with the $\pi 1/2^-[541] \otimes \nu 7/2^-[514]$ configuration. Therefore we propose that the dominant component of the ground-state band changes from $\pi 3/2^-[532] \otimes \nu 7/2^-[514]$ to $\pi 1/2^-[541] \otimes \nu 7/2^-[514]$ with increasing spin, which is consistent with the work of Sauvage *et al.* [22].

In Fig. 11(b), one can see that the quasiparticle alignment of band 1 increases gradually with increasing rotational frequency when the common Harris parameters are used. However, it is apparent that the two signature branches of band 1 show upbendings at the last few transitions, which should correspond to band crossings. The crossing frequencies in the $\alpha = 1$ and $\alpha = 0$ signatures are extracted to be $\hbar\omega \sim 0.32$ MeV and $\hbar\omega > 0.35$ MeV, respectively. Since the $h_{9/2}$ proton crossing is blocked, the alignment of a pair of $i_{13/2}$ neutrons should be responsible for the upbendings.

C. Band 2

Band 2 has been identified as the $\pi i_{13/2}(1/2^+[660]) \otimes \nu i_{13/2}(9/2^+[624])$ structure [6,23]. This kind of coupling (an $\Omega = 1/2$ decoupled orbital with a high-j intruder orbital, strongly affected by the Coriolis force) corresponds to a staggered semidecoupled structure, which displays a pronounced odd-even staggering reflecting the same phenomenon present in $\nu i_{13/2}$ bands. Similar semidecoupled bands have been observed in the neighboring odd-odd ^{176,178}Ir [33,38,39] and ^{182,186}Au [13,18] nuclei. One can see in Fig. 11(a) that band 2 experiences an apparent upbending at $\hbar\omega \simeq 0.25$ MeV, which has been attributed to the alignment of a $\pi h_{9/2}$ pair based on blocking arguments and measured $B(M1)/B(E2)$ ratios in our preliminary report [23]. Such a low-frequency $(\pi h_{9/2})^2$ alignment has also been proposed in the bands of several other Au isotopes in which an $i_{13/2}$ proton excitation is involved [2,3,11,13–15]. Generally, the alignment of an $h_{9/2}$ proton occurs at $\hbar\omega \geqslant 0.4$ MeV in this region, according to cranked shell model calculations [11]. However, the low-Ω $i_{13/2}$ proton drives the nucleus to a positive γ deformation ($\gamma \sim 10^\circ$) and reduces the proton pairing [11]. Both factors would favor the low-frequency $(\pi h_{9/2})^2$ alignment [11].

D. Band 3

Band 3 has been reported to be built on the $\pi h_{9/2} \otimes \nu 1/2^-[521]$ configuration [6]. Previously, the 68.6-keV, $I^\pi = 2^+$ isomeric state built on the $\pi h_{9/2} \otimes \nu 1/2^-[521]$ configuration [21] has been identified. Similar to the case of band 1, resonance ionization spectroscopy [29] reveals that the 2^+ isomeric state has a pure value of $K = 2$, which corresponds to the configuration $\pi 3/2^-[532] \otimes \nu 1/2^-[521]$ with $K = \Omega_p + \Omega_n = 2$. Semimicroscopic model calculations [22] suggest that the proton is predominately in the $\pi h_{9/2}$-$3/2^-[532]$ orbital for $I \leqslant 4$, whereas it is mainly in the $\pi h_{9/2}$-$1/2^-[541]$

orbital for $I > 4$ for the $\pi h_{9/2} \otimes \nu 1/2^-[521]$ configuration. Accepting the work of Sauvage *et al.* [22], we propose that band 3 built on the (5^+) state should be associated with the $\pi 1/2^-[541] \otimes \nu 1/2^-[521]$ configuration. This structure involves both a proton and a neutron predominantly in $\Omega = 1/2$ orbitals. Because of large signature splitting, the unfavored $\triangle I = 2$ transition sequences are normally difficult to observe.

The quasiparticle alignment versus rotational frequency for band 3 is shown in Fig. 11(a). With the help of three newly identified γ transitions, we observed the quasiparticle alignment of band 3 after the band crossing. As is clear in Fig. 11(a), band 3 experiences a pronounced upbending at $\hbar\omega \simeq 0.28$ MeV, which should be attributed to the neutron AB crossing. The neutron AB crossing frequencies for the $\pi 1/2^-[541]$ band in ^{183}Au and the $\nu 1/2^-[521]$ band in ^{183}Pt are 0.35 and 0.23 MeV, respectively, whereas it is 0.32 MeV for the ground-state band in ^{182}Pt. The crossing frequency in band 3 of ^{184}Au can be understood by the combined effect of the $\pi h_{9/2}$ band, which in ^{183}Au produces a delay, and the $\nu 1/2^-[521]$ band, which in ^{183}Pt decreases the crossing frequency with respect to the ground-state band of the even-even ^{182}Pt core. On the other hand, it is noted that the alignment gain for the neutron AB crossing in band 3 is about $4.2\hbar$, whereas the alignment gains in the $\pi 1/2^-[541]$ band of ^{183}Au and the $\nu 1/2^-[521]$ band of ^{183}Pt are about $5.7\hbar$ and $7.6\hbar$, respectively. The reduced alignment gain in band 3 with respect to the other two values in the $\pi 1/2^-[541]$ band of ^{183}Au and the $\nu 1/2^-[521]$ band of ^{183}Pt might be related to a deformation change effect.

As is well known, the doubly decoupled bands follow qualitatively the level spacings of the ground-state bands of the corresponding core nuclei. They cannot be understood with the $I(I+1)$ law but rather $R(R+1)$ must be used (where R is the collective angular momentum). This clear signature has allowed the identification of doubly decoupled $\pi 1/2^-[541] \otimes \nu 1/2^-[521]$ bands in several odd-odd Ir and Re nuclei. Following the method proposed in Ref. [40], we assume that the (5^+) state in band 3 of ^{184}Au has an expectation value $R_0 \neq 0$, and the collective angular momentum R increases in steps of two units along the band. R_0 and the rotational constant $A = \hbar^2/(2J)$ can be deduced from the first two transitions and used in turn to predict the upper ones. We obtained $R_0 = 1.38\hbar$ and $A = 13.98$ keV. The predicted ratios $X_I = (E_I - E_5)/(E_7 - E_5)$ are compared to the experimental values in Table III. One can see in Table III that the theoretical values agree well with experimental ones at low angular momenta. The deviation becomes more evident as spin increases; this might be associated with the combined effects of the softness of nuclei and the band crossing at high-spin states.

TABLE III. Experimental and calculated ratios $X_I = (E_I - E_5)/(E_7 - E_5)$ for the doubly decoupled band in ^{184}Au.

I	X_I^{exp}	X_I^{cal}
11	4.97	5.08
13	7.70	8.17
15	10.80	11.94
17	14.20	16.24
19	17.83	21.58

E. Band 4

Band 4 has been reported in a previous publication [6] where the quasiparticle configuration of $\pi h_{9/2} \otimes \nu i_{13/2}$ has been proposed. It is a well-known structure characterized as a semidecoupled band, which displays a pronounced odd-even staggering. Since band 4 was not connected to the ground state or known low-lying I^π states [21], the spin assignment for this band in the previous study [6] was partly based on the systematic comparison with the $\pi h_{9/2} \otimes \nu i_{13/2}$ structures observed in ^{182,184}Ir [41,42] and ^{186}Au [13]. However, the spin assignments for the latter three known bands are not unambiguous, and especially the deexcitation of the semidecoupled band for ^{186}Au [13] is not established. Therefore, it was natural to assign the $\triangle I = 2$ sequence with lower energy as the favored signature branch in ^{184}Au [6] before the low-spin signature inversion has been discovered by Bark *et al.* [43] in ^{162,164}Tm and ^{174}Ta. In the past fifteen years, a number of $\pi h_{9/2} \otimes \nu i_{13/2}$ bands observed in the odd-odd Tm, Lu, Ta, Re, Ir, and Au isotopes have been reported to show the low-spin signature inversion phenomenon. Further systematic studies show [19,20,44] that the low-spin signature inversion is a common feature for the $\pi h_{9/2} \otimes \nu i_{13/2}$ bands. According to systematic studies [19,20], a one-unit increment in spins of band 4 with respect to the original ones [6] has been adopted in the present work.

In studies of the β^+/EC decay of ^{184}Hg [21,22], the 228.4-keV, $I^\pi = 3^-$ and 254.3-keV, $I^\pi = 2^-$ states have been identified as the $\pi 3/2^-[532] \otimes \nu 9/2^+[624]$ and $\pi 3/2^-[532] \otimes \nu 7/2^+[633]$ configurations, respectively. The existence of the two low-lying states indicates that the proton is mainly in the $\pi h_{9/2}$-$3/2^-[532]$ orbital and the $\nu i_{13/2}$-$7/2^+[633]$ configuration would compete with the $\nu i_{13/2}$-$9/2^+[624]$ configuration at low-spin states. For the $\pi h_{9/2} \otimes \nu 7/2^-[514]$ and $\pi h_{9/2} \otimes \nu 1/2^-[521]$ configurations discussed in Sec. III B and Sec. III D, the proton is mainly in the $\pi h_{9/2}$-$3/2^-[532]$ orbital at low-spin states and moves into the $\pi h_{9/2}$-$1/2^-[541]$ orbital at high-spin states. Similarly, one may expect that the proton is predominately in the $\pi h_{9/2}$-$1/2^-[541]$ orbital in band 4. On the other hand, it should be noted that $\nu i_{13/2}$-$9/2^+[624]$ is closer to the neutron Fermi surface than $\nu i_{13/2}$-$7/2^+[633]$ in the $N = 105$ isotones. The $\nu i_{13/2}$-$9/2^+[624]$ bands in both the ^{183}Pt [4] and ^{185}Hg [5] nuclei have been strongly populated in heavy-ion-induced fusion-evaporation reactions. Therefore $\nu i_{13/2}$-$9/2^+[624]$ is suggested to be the main component in band 4. Based on the above-mentioned arguments, we propose that band 4 should be described by the configuration $\pi 1/2^-[541] \otimes \nu 9/2^+[624]$. The deduced experimental $B(M1)/B(E2)$ ratios versus spin I are plotted and compared with theoretical predications in Fig. 10(b). Good agreement is obtained under the assumption of this configuration.

The plots of quasiparticle alignment of band 4 versus the rotational frequency are shown in Fig. 11(a). One can see that the alignments of two $\triangle I = 2$ signature branches of band 4 cross twice at two certain frequencies when the common Harris parameters are used. The first crossing could be attributed to signature-dependent deformations [4,45], while the second one should be due to different band-crossing frequencies of the two signature branches. Another dramatic feature of band 4 is that the $\alpha = 0$ sequence shows a sharp rise in alignment at $\hbar\omega = 0.32$ MeV, while the $\alpha = 1$ sequence displays a rather smooth behavior for the whole range of rotational frequencies. Similarly, one can see in Fig 11(d) that the upbending occurs more sharply in the $\alpha = -1/2$ sequence than that in the $\alpha = +1/2$ sequence of the $\nu i_{13/2}$ band in ^{183}Pt. In fact, for the $\pi h_{9/2} \otimes \nu i_{13/2}$ band, the odd proton occupies the favored orbital with the signature $\alpha_f^p = +1/2$, and the odd neutron could occupy both the favored and unfavored orbitals ($\alpha^n = \pm 1/2$). According to the signature additive rule, the $\alpha_f = 1$ and $\alpha_{uf} = 0$ signatures of the $\pi h_{9/2} \otimes \nu i_{13/2}$ configuration correspond to the $\alpha_f = +1/2$ and $\alpha_{uf} = -1/2$ signatures of the $\nu i_{13/2}$ configuration, respectively. Therefore, it is reasonable that the quasiparticle alignments of the $\pi h_{9/2} \otimes \nu i_{13/2}$ band in ^{184}Au and the $\nu i_{13/2}$ band in ^{183}Pt behave similarly.

Obviously, the $\alpha = 0$ sequence of band 4 experiences a band crossing at $\hbar\omega \approx 0.32$ MeV. Due to its unique configuration, both the proton ef and neutron AB crossings are blocked. The band crossing in the $\alpha = 0$ signature should be associated with the neutron AD alignment. One may expect that the the AD crossing in band 4 should be delayed with respect to the AB crossing in band 1. However, the observed AD crossing in the $\pi h_{9/2} \otimes \nu i_{13/2}$ band (band 4) and the AB crossing in the $\pi h_{9/2} \otimes \nu 7/2^-[514]$ band (band 1) occur at approximately the same rotational frequency. To understand this phenomenon, we refer to the theoretical work reported in Refs. [4,11,46]. Total Routhian surface calculations have shown that an $i_{13/2}$ quasineutron could drive the nucleus from axially symmetric to a triaxial shape with slightly smaller β_2 and large negative γ up to -12° [4]. Both factors would enhance the action of the Coriolis force on the pair of $i_{13/2}$ neutrons and reduce the AD crossing frequency. The two factors have been successfully applied to explain the experimental result that the AD crossing frequency in the $\nu i_{13/2}$ band is close to the AB crossing frequency in the $7/2^-[514]$ band of ^{183}Pt [4]. Similarly, the reduced AD crossing frequency in the $\pi h_{9/2} \otimes \nu i_{13/2}$ band of ^{184}Au could be attributed to the smaller β_2 and more negative-γ driving effects of the $\nu i_{13/2}$ orbital.

For the deformed rare-earth nuclei, the occupation of the $\pi 1/2^-[541](h_{9/2})$ intruder orbital by a quasiproton is usually considered to drive the nucleus toward larger quadrupole deformation and lead to a delayed band-crossing frequency [47]. However, the Fermi surface enters into the proton $h_{9/2}$ subshell in Au nuclei and the deformation driving effects of the $\pi 1/2^-[541]$ orbital vanish. If the deformation driving effects of the $\pi 1/2^-[541]$ intruder orbital are negligible and have no obvious influence on band-crossing frequencies, the neutron AD crossing in both the $\pi 1/2^-[541] \otimes \nu i_{13/2}$ band of ^{184}Au and the $\nu i_{13/2}$ band of ^{183}Pt should occur at a similar frequency. However, the experimental AD crossing frequencies are extracted to be $\hbar\omega_c \approx 0.32$ and 0.27 MeV in the $\pi 1/2^-[541] \otimes \nu i_{13/2}$ band of ^{184}Au and the $\nu i_{13/2}$ band of ^{183}Pt [4], respectively. The theoretical calculations predict (see, for example, Refs. [2,11]) that the nucleus has roughly constant deformations of $\beta_2 \sim 0.23$ and $\gamma \geqslant 0^\circ$ when the proton intruder orbital $1/2^-[541]$ is occupied and the positive γ deformation would delay the neutron AD crossing [4]. The coupling of the $1/2^-[541]$ proton to the $i_{13/2}$ neutron would lead to less negative γ deformation in comparison with the single $i_{13/2}$ neutron. Correspondingly, the $\hbar\omega(AD)$ in the $\pi 1/2^-[541] \otimes \nu i_{13/2}$ band of ^{184}Au becomes larger than that in the $\nu i_{13/2}$ band of ^{183}Pt. The stabilization effects of $1/2^-[541]$ proton excitation are reflected by the decreasing signature splitting in the $\pi 1/2^-[541] \otimes \nu i_{13/2}$ band of ^{184}Au as compared to the $\nu i_{13/2}$ band of ^{183}Pt. In fact, the signature splittings in both bands originate from the $i_{13/2}$ neutron. A large negative γ deformation caused by the $i_{13/2}$ neutron leads to an enhanced signature splitting [4], whereas the $1/2^-[541]$ proton stabilizes the nucleus against γ deformation. Consequently, the signature splitting becomes smaller in the $\pi 1/2^-[541] \otimes \nu i_{13/2}$ two-quasiparticle band.

In addition, we would like to mention that the $\nu i_{13/2}$ crossing frequency is directly proportional to the quadrupole deformation according to cranked shell model calculations [11]. Since the low-Ω $i_{13/2}$ proton could drive the nucleus toward larger quadrupole deformation in comparison with the low-Ω $h_{9/2}$ proton based on both theoretical and experimental investigations [2,11,18,48,49], the $\nu i_{13/2}$ crossing frequency in the $\pi i_{13/2} \otimes \nu i_{13/2}$ band would be delayed with respect to the $\pi h_{9/2} \otimes \nu i_{13/2}$ band. An inspection of Fig. 11(a) reveals that the crossing frequency in the $\pi i_{13/2} \otimes \nu i_{13/2}$ band (band 2) is much lower than that in the $\pi h_{9/2} \otimes \nu i_{13/2}$ band (band 4), which in turn suggests that the band crossing in band 2 is not $\nu i_{13/2}$ but $\pi h_{9/2}$ crossing.

F. Band 5

Band 5 shows strong $E2$ crossing cascade transitions and weak in-band $M1/E2$ transitions (see Fig. 1) and displays small signature splitting before band crossing. According to the discussion in Sec. II B, band 5 has been assigned as a negative-parity band. As is shown in Fig. 9, there are three candidates, i.e., $\pi 1/2^+[660] \otimes \nu 1/2^-[521]$, $\pi 1/2^+[660] \otimes \nu 7/2^-[514]$, and $\pi 11/2^-[505] \otimes \nu 9/2^+[624]$. The $\pi 1/2^+[660] \otimes \nu 1/2^-[521]$ and $\pi 11/2^-[505] \otimes \nu 9/^+[624]$ configurations could be excluded, since they correspond to doubly decoupled and strongly coupled band structures, respectively, which are not consistent with the character of band 5. Consequently, the $\pi 1/2^+[660] \otimes \nu 7/2^-[514]$ configuration should be responsible for band 5. This configuration assignment is further validated according to the following considerations: (i) One can see in Fig. 12 that the kinematical moment of inertia of band 5 is rather large. It follows the trend of the $\pi 1/2^+[660] \otimes \nu i_{13/2}$ band in ^{184}Au and the $\pi 1/2^+[660]$ band in ^{183}Au, which implies the presence of the $\pi 1/2^+[660]$ orbital in the intrinsic structure of band 5. (ii) In Fig. 10(c), we compare the theoretical estimates of the $B(M1)/B(E2)$ ratios for the $\pi 1/2^+[660] \otimes \nu 7/2^-[514]$ configuration with the experimental ones, and the results are in good agreement. Based on the arguments mentioned above, we propose the $\pi 1/2^+[660] \otimes \nu 7/2^-[514]$ configuration for band 5. In fact,

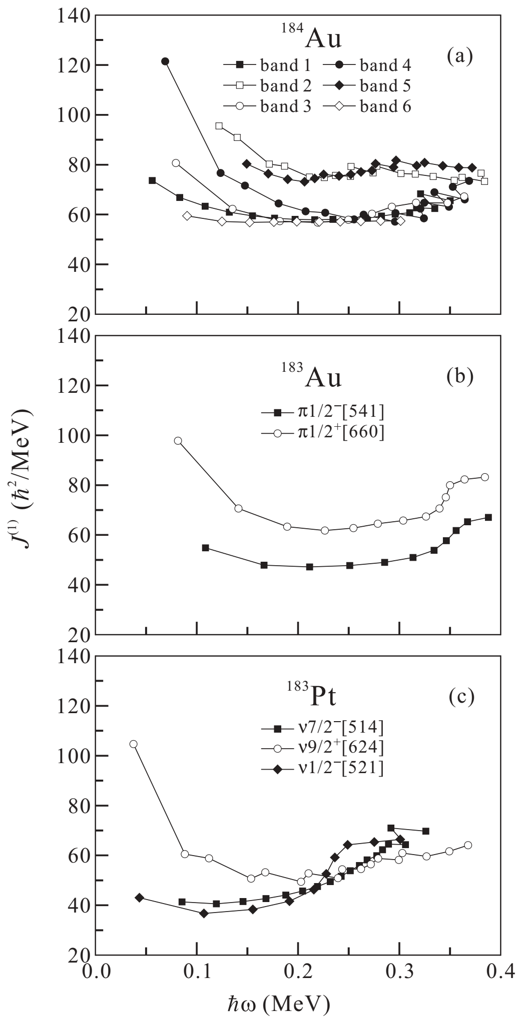

FIG. 12. Experimental kinematical moments of inertia as a function of rotational frequency for prolate bands in ^{184}Au and neighboring nuclei.

the proton $i_{13/2}$-$1/2^+[660]$ bands are yrast in the neighboring odd-Z nuclei [2,3]. The $7/2^-[514]$ bands in ^{183}Pt [4] and ^{185}Hg [5] have been observed to be low lying and intensely populated in the heavy-ion-induced fusion-evaporation reactions. Consequently, the two-quasiparticle band built on the $\pi 1/2^+[660] \otimes \nu 7/2^-[514]$ configuration is expected to be easily populated in the (HI, xn) reaction used in this experiment.

One can see in Fig. 11(a) that band 5 has an initial alignment as high as $\sim 8\hbar$ at $\hbar\omega \approx 0.15$ MeV. This is consistent with the configuration assignment; the low-Ω $i_{13/2}$ proton contributes about $6\hbar$, while the rest originates from the $7/2^-[514]$ neutron. As is seen in Fig 11(a), band 5 has a clear alignment process at $\hbar\omega \simeq 0.26$ MeV, with an alignment gain of $6\hbar$. Since neither neutron AB alignment nor proton ef alignment is blocked in the $\pi i_{13/2} \otimes \nu 7/2^-[514]$ band, both alignment processes might be observed in band 5. As pointed out in Sec. III B, the upbending in the alignment of the $\pi h_{9/2} \otimes \nu 7/2^-[514]$ band (band 1) at $\hbar\omega \sim 0.32$ MeV has been attributed to the neutron AB alignment because the proton ef alignment is blocked. For the $\pi i_{13/2} \otimes \nu 7/2^-[514]$ band, the associated proton is changed from $1/2^-[541](h_{9/2})$ to $1/2^+[660](i_{13/2})$. It is thus reasonable to conclude that the alignment of a $\pi h_{9/2}$ pair plays a crucial role in the band crossing of band 5. We have noted that the alignment gain in band 5 is larger than that in band 2. The band crossing in band 2 has been attributed to the alignment of a $\pi h_{9/2}$ pair with an alignment gain of $3.5\hbar$. If the alignment of band 5 is totally due to the alignment of a pair of $\pi h_{9/2}$ protons, one wonders why the alignment gain for such a pair is as high as $6\hbar$ in band 5 while it is only of 3.5 units in band 2. Mueller *et al.* [2] suggested that the upbending observed in the ground-state band of ^{182}Pt and the $\pi i_{13/2}$ band of ^{183}Au below $\hbar\omega = 0.30$ MeV result from simultaneous alignments of the $(h_{9/2})^2$ protons and the $(i_{13/2})^2$ neutrons at degenerate frequencies. If this mechanism is applied to band 5, another problem arises; that is, the alignment gain is as high as $9\hbar$ in the ground-state band of ^{182}Pt and the $\pi i_{13/2}$ band of ^{183}Au, which is much larger than the value in band 5. An alternative explanation could be adopted. If we keep an alignment gain of 3.5 units for the $\pi h_{9/2}$ pair in ^{184}Au, the remaining $\triangle i_x = 2.5\hbar$ in the $\pi i_{13/2} \otimes \nu 7/2^-[514]$ band could be due to a weak alignment of a $\nu i_{13/2}$ pair. A similar phenomenon has been reported in the $\pi i_{13/2}$ band of ^{187}Au by Bourgeois *et al.* [15].

G. Band 6

Band 6 shows intense in-band $M1/E2$ transitions [see Figs. 1 and 7(a)] and no signature splitting, which are consistent with the character of the strongly coupled structure. The strong $M1/E2$ transitions indicate a high-K and/or a large-g_K factor involved in this band. We have noticed that no analogous structures have been observed so far in the odd-odd Au nuclei. Band 6 exhibits a value of 10.2 for the $K_{\rm eff}$ parameter. This parameter corresponds to an effective projection quantum number K and is obtained as follows: From the expression for the energies of the states belonging to a rotational band,

$$E(I) = E_0 + \frac{\hbar^2}{2J}[I(I+1) - K^2], \tag{10}$$

one calculates the ratio between the first two $\triangle I = 1$ transitions [30] to be

$$x = \frac{E(K+2) - E(K+1)}{E(K+1) - E(K)} = \frac{K+2}{K+1} \tag{11}$$

and a K value, denoted $K_{\rm eff}$, is extracted as

$$K_{\rm eff} = \frac{2-x}{x-1}. \tag{12}$$

The high value of $K_{\rm eff}$ obtained for band 6 indicates that the band is not compressed; this corresponds to the case in which both proton and neutron orbitals are weakly affected by the Coriolis interaction, resulting in $K_{\rm eff} \approx K = \Omega_p + \Omega_n$ [33]. Therefore, the presence of the $\pi h_{9/2}$, $\pi i_{13/2}$, and $\nu i_{13/2}$ orbitals could be excluded [33]. Given the calculated zero-order level scheme shown in Fig. 9, the $\pi 11/2^-[505] \otimes \nu 7/2^-[514]$ configuration is the only candidate which satisfies the above conditions. In addition, this configuration could give rise to a strongly coupled structure. Therefore, we propose the $\pi 11/2^-[505] \otimes \nu 7/2^-[514]$ ($K^\pi = 9^+$) configuration for band 6. Correspondingly, the spin and parity for the lowest level of the band have been assigned to be $I_0^\pi = K^\pi = (9^+)$. Furthermore, one can see in Fig. 10(d) that the experimental $B(M1)/B(E2)$ ratios are fairly well reproduced under the assumption of the $\pi 11/2^-[505] \otimes \nu 7/2^-[514]$ configuration. Similar strongly coupled bands built on the $\pi h_{11/2} \otimes \nu 7/2^-[514]$ configuration have been identified in the neighboring odd-odd ^{178,180}Ta [50,51], ^{180}Re [52], and ^{178}Ir [33] nuclei.

One can see in Fig. 11(b) that band 6 shows alignment gain from $\sim 3.1\hbar$ at low rotational frequency up to $\sim 6.7\hbar$ at the highest measured rotational frequency when the common Harris parameters are used; no backbending has been observed. The complex alignment pattern is very interesting and needs further explanations; this is beyond the scope of this paper.

H. Band 7

Two quasiparticle bands built on the oblate $\pi h_{11/2}^{-1} \otimes \nu i_{13/2}^{-1}$ configuration with bandhead $I^\pi = 11^-$ have been systematically observed in the odd-odd $^{186\text{–}194}$Au nuclei [13,53–59]. (Note that we write $\pi^- \otimes \nu^-$ and $\pi \otimes \nu$ for hole and particle configurations, respectively.) These bands are thought to result from the proton- and neutron-hole excitations coupled to corresponding even-even Hg cores. We have noted that band 7 of ^{184}Au displays a striking similarity to those oblate $\pi h_{11/2}^{-1} \otimes \nu i_{13/2}^{-1}$ bands in $^{186\text{–}194}$Au. Figure 13 presents the level schemes of band 7 in ^{184}Au and the $\pi h_{11/2}^{-1} \otimes \nu i_{13/2}^{-1}$ bands in $^{186\text{–}194}$Au for a comparison. Based on the systematic progression of these bands as a function of neutron number, we propose the oblate $\pi h_{11/2}^{-1} \otimes \nu i_{13/2}^{-1}$ configuration for band 7 and assign spin-parity (11^-) to the bandhead.

For a near-oblate-shaped nucleus in this mass region, the proton and neutron Fermi levels lie at the upper $\pi h_{11/2}$ and middle-to-upper $\nu i_{13/2}$ subshells, respectively, close to the low-Ω orbitals of these subshells. The $\pi h_{11/2}^{-1}$ band in ^{185}Au and $\nu i_{13/2}^{-1}$ band in ^{185}Hg have been identified to be decoupled bands [3,5], where both proton and neutron holes are considered to be mainly in the $\Omega = 1/2$ orbitals [3,60]. Therefore the $\pi h_{11/2}^{-1}$ band coupled to the $\nu i_{13/2}^{-1}$ band would result in $K \sim 0$. Figure 14 presents the quasiparticle alignments i_x versus rotational frequency for the oblate $\pi h_{11/2}^{-1}$ (^{185}Au), $\nu i_{13/2}^{-1}$ (^{185}Hg), and $\pi h_{11/2}^{-1} \otimes \nu i_{13/2}^{-1}$ (^{184}Au) bands. For the $\pi h_{11/2}^{-1} \otimes \nu i_{13/2}^{-1}$ configuration, $K = 0$ has been used for calculations. The $\pi h_{11/2}^{-1}$ band has an initial alignment of $i_p \approx 4.5\hbar$ and the $\nu i_{13/2}^{-1}$ band shows $i_n \approx 6.3\hbar$. The resultant sum $i_{pn}^{\text{cal}} = i_p + i_n \approx 10.8\hbar$ agrees well with the observed large initial alignment of $i_{pn}^{\text{exp}} \simeq 10.7\hbar$ for the $\pi h_{11/2}^{-1} \otimes \nu i_{13/2}^{-1}$

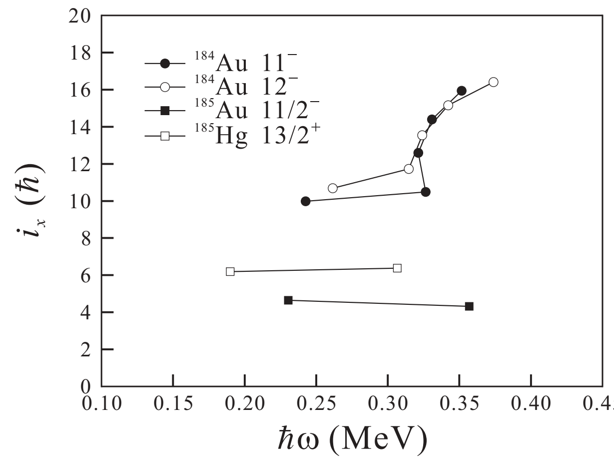

FIG. 14. Aligned angular momenta i_x as a function of rotational frequency for the oblate bands with the common reference $J_0 = 8\hbar^2\,\text{MeV}^{-1}$, $J_1 = 40\hbar^4\,\text{MeV}^{-3}$.

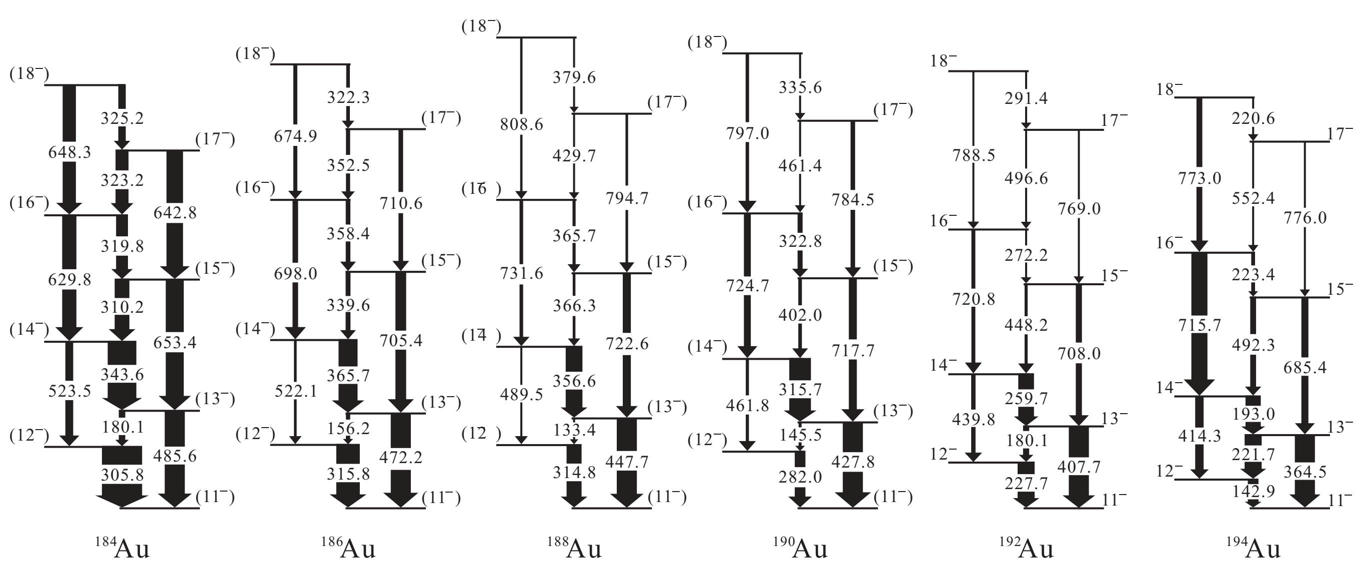

FIG. 13. Band structures built on the $\pi h_{11/2}^{-1} \otimes \nu i_{13/2}^{-1}$ configuration in odd-odd $^{184\text{–}194}$Au. The data sources are ^{184}Au (this work), ^{186}Au [13,53], ^{188}Au [13,54], ^{190}Au [55,57], ^{192}Au [55], and ^{194}Au [55,58]. The relative intensities are normalized to the $13^- \to 11^-$ transitions, respectively.

configuration in ^{184}Au, which is consistent with the presence of the proposed orbitals.

In Fig. 14, it is clear that the $\pi h_{11/2}^{-1} \otimes \nu i_{13/2}^{-1}$ band shows an apparent upbending at $\hbar\omega \approx 0.33$ MeV with an alignment gain of about $5.5\hbar$. This number is somewhat uncertain since the crossing is not complete at the highest lying transitions. The sharp upbending corresponds to the second $\nu i_{13/2}$ crossing since the first $\nu i_{13/2}$ crossing is blocked. It is worth noting that the second $\nu i_{13/2}$ crossing frequency is observed in the oblate $\nu i_{13/2}^{-1}$ bands of odd-A Hg isotopes at approximately 0.27 MeV [61–64], which is much smaller than the value of 0.33 MeV in the $\pi h_{11/2}^{-1} \otimes \nu i_{13/2}^{-1}$ band of ^{184}Au. The band-crossing frequency in the $\pi h_{11/2}^{-1} \otimes \nu i_{13/2}^{-1}$ band of ^{188}Au has been determined to be 0.31 MeV [13]. In Ref. [13], Janzen *et al.* have qualitatively attributed the different crossing frequencies between the $\pi h_{11/2}^{-1} \otimes \nu i_{13/2}^{-1}$ band of ^{188}Au and the $\nu i_{13/2}^{-1}$ bands of odd-A Hg isotopes to the difference of γ deformations [13], where the γ deformation of the $\pi h_{11/2}^{-1} \otimes \nu i_{13/2}^{-1}$ band is more negative than $\gamma = -60^\circ$ and the γ deformation of the $\nu i_{13/2}^{-1}$ band is less negative than $\gamma = -60^\circ$. It seems the same mechanism could be applied to the case of ^{184}Au.

I. Signature inversion in the prolate $\pi h_{9/2} \otimes \nu i_{13/2}$ and $\pi i_{13/2} \otimes \nu i_{13/2}$ bands of ^{184}Au

With the information provided in this article, one can further investigate the characteristics of signature splitting and signature inversion for the observed rotational bands in ^{184}Au. The signature splitting $\triangle e'$ is defined as the energy difference at a given rotational frequency for the pair of signature partners. In the present work, we used the quantity

$$S(I) = E(I) - E(I-1) - \tfrac{1}{2}[E(I+1) - E(I) + E(I-1) - E(I-2)] \tag{13}$$

instead of $\triangle e'$. Here $E(I)$ is the level energy of state I; $S(I)$ is directly proportional to the signature splitting $\triangle e'$, but it is magnified by approximately a factor of 2.

For an odd-odd nucleus, the signature-splitting amplitude of a given rotational band is mainly determined by the quasiparticle orbital which has smaller splitting amplitude in the corresponding odd-A nucleus. For the observed $\pi h_{9/2} \otimes \nu i_{13/2}$ and $\pi i_{13/2} \otimes \nu i_{13/2}$ bands in ^{184}Au, the odd proton always occupies the favored orbitals with the signature $\alpha_f^p = +1/2$ due to the large signature splittings of the low-Ω, high-j orbitals $h_{9/2}(1/2^-[541])$ and $i_{13/2}(1/2^+[660])$. Both favored and unfavored orbitals can be occupied by the $i_{13/2}$ quasineutron. Therefore, the signature splitting is entirely due to the $i_{13/2}$ quasineutron orbital for both rotational bands. For the two configurations, the expected favored signatures are $\alpha_f^{p\text{-}n} = \alpha_f^p + \alpha_f^n = 1/2 + 1/2 = 1$ (odd-spin sequences), and the unfavored signatures are $\alpha_{uf}^{p\text{-}n} = \alpha_f^p + \alpha_{uf}^n = 1/2 - 1/2 = 0$ (even-spin sequences).

Figure 15 presents the plots of the signature splittings for the $\pi h_{9/2} \otimes \nu i_{13/2}$ and $\pi i_{13/2} \otimes \nu i_{13/2}$ bands of ^{184}Au. Obviously, both bands exhibit apparent signature splittings at low- and medium-spin states. From a closer inspection of Fig. 15, one can find that the signature-splitting amplitude in the $\pi i_{13/2} \otimes \nu i_{13/2}$ band is reduced with respect to the value in the $\pi h_{9/2} \otimes \nu i_{13/2}$ band. A similar phenomenon has also been observed in ^{176,178}Ir [33,38,39] and ^{182,186}Au [13,18]. As pointed out before, the signature splitting of both bands is determined by the $i_{13/2}$ quasineutron orbital. It is well known that the signature splitting can be interpreted as arising from a mixture of the $\nu 1/2^+[660](i_{13/2})$ component into the wave function [65,66]. Thus the amplitude of signature splitting depends on the distance of the neutron Fermi surface with respect to the $\nu 1/2^+[660](i_{13/2})$ Nilsson orbital. If the neutron Fermi surface is far from the $\nu 1/2^+[660]$ orbital, the mixing of the $\nu 1/2^+[660]$ component into the wave function should be small. Correspondingly, the signature splitting would be small. Since the $\pi 1/2^+[660](i_{13/2})$ proton drives the nucleus toward a larger quadrupole deformation, the $\nu 1/2^+[660]$ orbital is moved further from the neutron Fermi surface in the Nilsson diagrams. Simultaneously, because of the large kinematical moment of inertia associated with the $\pi i_{13/2} \otimes \nu i_{13/2}$ configuration, the Coriolis effect should be weaker, which would also lead to reduced signature splitting [66]. Therefore, the smaller signature splitting in the $\pi i_{13/2} \otimes \nu i_{13/2}$ band in comparison with that in the $\pi h_{9/2} \otimes \nu i_{13/2}$ band could be qualitatively attributed to the larger quadrupole deformation in the former band.

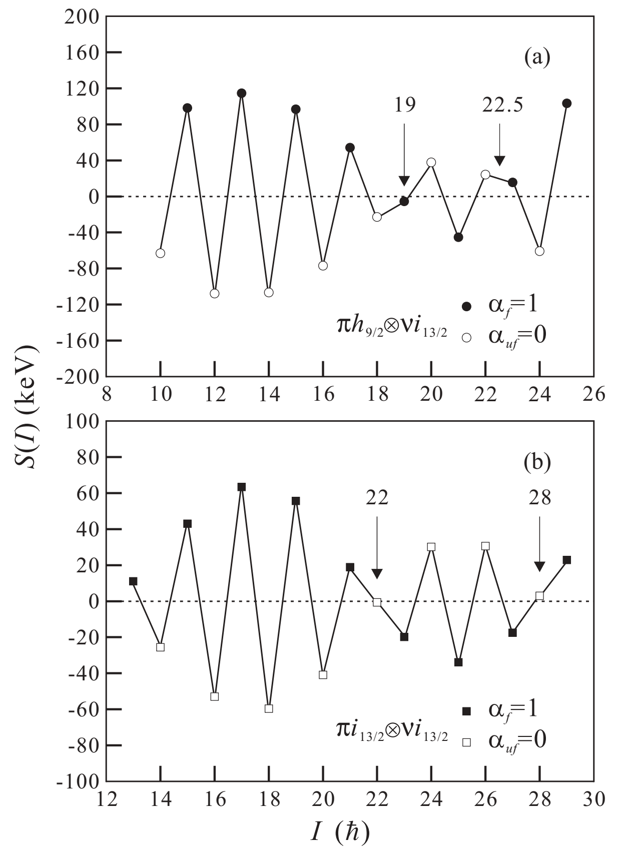

FIG. 15. Experimental signature splittings $S(I)$ vs I for the $\pi h_{9/2} \otimes \nu i_{13/2}$ and $\pi i_{13/2} \otimes \nu i_{13/2}$ bands observed in ^{184}Au. The filled symbols indicate $\triangle I = 2$ favored signature branches ($\alpha_f = 1$), and the open symbols correspond to the unfavored ones ($\alpha_{uf} = 0$).

One can see in Fig. 15 that the similar staggering pattern of the $\pi h_{9/2} \otimes \nu i_{13/2}$ and $\pi i_{13/2} \otimes \nu i_{13/2}$ bands is interesting; i.e.,

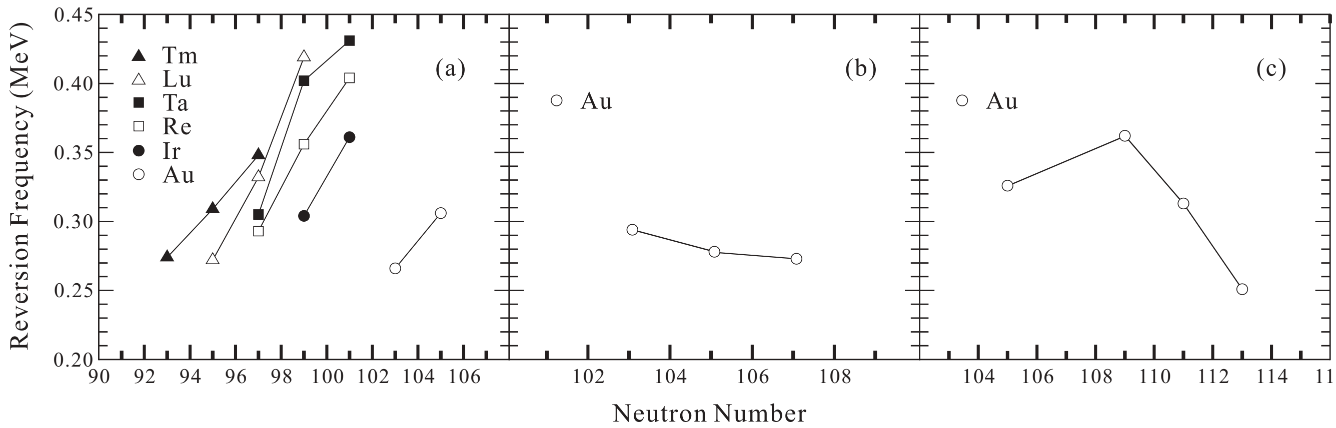

FIG. 16. Reversion frequency, as defined in the text, for (a) the $\pi h_{9/2} \otimes \nu i_{13/2}$ bands in the $A \approx 170$ region, (b) the $\pi i_{13/2} \otimes \nu i_{13/2}$ bands in the Au isotopes, and (c) the oblate $\pi h_{11/2}^{-1} \otimes \nu i_{13/2}^{-1}$ bands in the Au isotopes. The data sources are ^{162,164}Tm [43], ^{166}Tm [69], ^{166}Lu [70], ^{168}Lu [71,72], ^{170}Lu [73], ^{170}Ta [44,74], ^{172}Ta [75], ^{174}Ta [43], ^{172}Re [19], ^{174}Re [76], ^{176}Re [77], ^{176}Ir [38,39], ^{178}Ir [33], ^{182}Au [18], ^{184}Au (this work), ^{186}Au [13,26], ^{188}Au [13,54], ^{190}Au [55,57], and ^{192}Au [55,59].

the unfavored signature branch is energetically favored rather than the favored signature sequence at low- and medium-spin states. Such a behavior has been referred to as the low-spin signature inversion or anomalous signature splitting [16]. With increasing angular momentum, the inverted signature splitting decreases and the two signature branches cross with each other at $I^\pi = 19^-$ and $I^\pi = 22^+$ for the $\pi h_{9/2} \otimes \nu i_{13/2}$ and $\pi i_{13/2} \otimes \nu i_{13/2}$ bands, respectively. Beyond the inversion spin at which the two signature branches cross, normal signature splitting is observed in both bands. The observation of the inversion spin provides supplementary evidence for low-spin signature inversion [19]. Another interesting feature worth noting is that the signature splitting starts getting reinverted again beyond $I^\pi = 22.5^-$ in the $\pi h_{9/2} \otimes \nu i_{13/2}$ band of ^{184}Au. A careful analysis of the signature splittings for all the observed $\pi h_{9/2} \otimes \nu i_{13/2}$ bands to date reveals that ^{184}Au is the only case which displays such a second signature inversion phenomenon. One can see in Fig. 11(a) that the neutron *BC* crossing is delayed with respect to the neutron *AD* crossing in the $\pi h_{9/2} \otimes \nu i_{13/2}$ band, which might be associated with the second signature inversion observed in this band. Similarly, a second signature inversion seems to occur beyond $I^\pi = 28^+$ in the $\pi i_{13/2} \otimes \nu i_{13/2}$ band of ^{184}Au. However, the level staggering pattern beyond the second signature inversion has not been well established in this experiment; further experimental study is needed to extend this band up to higher spin states and check whether the second signature inversion does really exist.

Previous studies of odd-odd nuclei in the $A \approx 170$ region have established a consistent pattern of signature splitting for a number of $\pi h_{9/2} \otimes \nu i_{13/2}$ bands. Systematic studies and analyses have been made in several recent publications (see, for example, Refs. [19,20,44]). The inversion spin is a useful tool for systematic discussions of low-spin signature inversion. However, it is known that the level spins in odd-odd nuclei are not usually confidently assigned. Therefore, the inversion spin cannot be exactly extracted for most of the $\pi h_{9/2} \otimes \nu i_{13/2}$ bands. In this paper, we preferred to use the reversion frequency for discussion. For a given two-quasiparticle rotational band in an odd-odd nucleus, the reversion frequency is the frequency where the Routhians of the $\alpha = 0$ and $\alpha = 1$ sequences cross and below which signature inversion is observed [17,67]. As discussed in Ref. [67], this frequency is not terribly dependent on the spin assignment. The reversion frequencies for the $\pi h_{9/2} \otimes \nu i_{13/2}$ bands in the $A \approx 170$ region are displayed in Fig. 16(a). Inspecting Fig. 16(a), one sees that the reversion frequency increases with increasing the neutron number for the given isotope chains of Tm, Lu, Ta, Re, and Ir, which has also been pointed out in Ref. [44]. The reversion frequencies for the $\pi h_{9/2} \otimes \nu i_{13/2}$ bands of ^{182,184}Au have been extracted to be 0.266 and 0.306 MeV, respectively, while this frequency for ^{186}Au is not observed up to the measured rotational frequency $\hbar\omega = 0.369$ MeV [68]. The three nuclei of ^{182,184,186}Au fit well into the above-mentioned systematic expectation; i.e., the reversion frequency increases with increasing neutron number. However, ^{188}Au does not follow the trend. The reversion frequency for ^{188}Au [54], which is not shown in Fig. 16(a), is determined to be 0.282 MeV. This value is at least 0.087 MeV smaller than that for ^{186}Au. Total Routhian surface calculations [54] showed that there is a large deformation change between ^{188}Au and ^{186}Au; this should be responsible for the anomaly. Figure 16(b) presents the reversion frequencies for the $\pi i_{13/2} \otimes \nu i_{13/2}$ bands in the Au isotopes. It is clear that the reversion frequency decreases with increasing neutron number in ^{182,184,186}Au. In fact, the reversion frequency for the $\pi i_{13/2} \otimes \nu i_{13/2}$ band of ^{178}Ir [38] is determined to be 0.283 MeV, while this frequency for ^{176}Ir is not observed up to the measured rotational frequency $\hbar\omega = 0.424$ MeV [38]. Focusing on the two isotope chains comprising ^{176,178}Ir and ^{182,184,186}Au, we note that the changes of the reversion frequency versus neutron number for the $\pi i_{13/2} \otimes \nu i_{13/2}$ configuration are opposite to the trend for the $\pi h_{9/2} \otimes \nu i_{13/2}$ configuration.

The low-spin signature inversion in the $\pi h_{9/2} \otimes \nu i_{13/2}$ and $\pi i_{13/2} \otimes \nu i_{13/2}$ bands of ^{176,178}Ir has been investigated in the framework of the two-quasiparticle plus rotor model [33,38]; it has been determined that a residual proton-neutron interaction was necessary to produce the low-spin signature inversion.

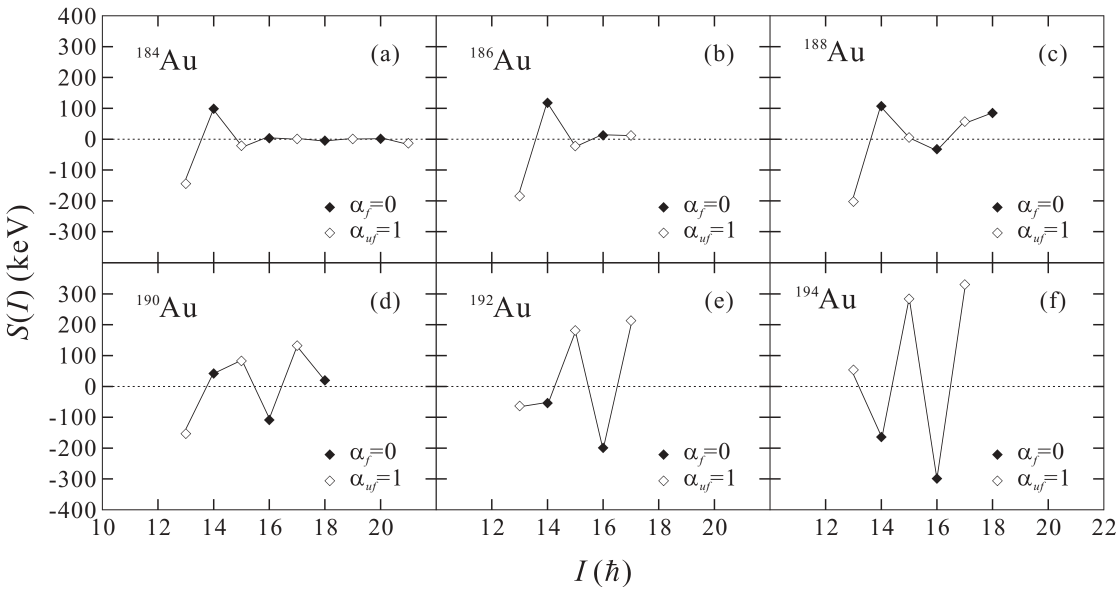

FIG. 17. Signature splittings $S(I)$ as a function of spin I for the oblate $\pi h_{11/2}^{-1} \otimes \nu i_{13/2}^{-1}$ bands in doubly odd Au nuclei: ^{184}Au (this work), ^{186}Au [13], ^{188}Au [13,54], ^{190,192}Au [55,56], and ^{194}Au [55,58]. The filled and open symbols correspond to the signature-favored ($\alpha_f = 0$) and signature-unfavored ($\alpha_{uf} = 1$) levels, respectively.

The extended total Routhian surface calculations showed that quadrupole pairing plays a role in generating the low-spin signature inversion in the $\pi h_{9/2} \otimes \nu i_{13/2}$ and $\pi i_{13/2} \otimes \nu i_{13/2}$ bands of ^{182}Au [18]. It seems that both theoretical approaches give reasonable descriptions of signature inversion for some selected cases. In this sense, a reproduction of low-spin signature inversion in the $\pi h_{9/2} \otimes \nu i_{13/2}$ and $\pi i_{13/2} \otimes \nu i_{13/2}$ bands of ^{184}Au may be crucial for a full understanding of the inversion mechanism.

J. Signature inversion in the oblate $\pi h_{11/2}^{-1} \otimes \nu i_{13/2}^{-1}$ bands of ^{184}Au and neighbors

For the oblate $\pi h_{11/2}^{-1} \otimes \nu i_{13/2}^{-1}$ configuration, the signature splitting is determined by the $i_{13/2}$ quasineutron orbital [13]. The $h_{11/2}$ quasiproton contributes a favored signature ($\alpha_f^p = -1/2$) while both favored and unfavored signatures are involved for the $i_{13/2}$ quasineutron. Therefore, the quasineutron occupation of the favored orbital ($\alpha_f^n = +1/2$) leads to the favored branch with $\alpha_f^{p\text{-}n} = \alpha_f^p + \alpha_f^n = 0$, while the quasineutron unfavored orbital ($\alpha_{uf}^n = -1/2$) defines the unfavored branch with $\alpha_{uf}^{p\text{-}n} = |\alpha_f^p + \alpha_{uf}^n| = 1$. Figure 17 presents plots of the signature splittings for the $\pi h_{11/2}^{-1} \otimes \nu i_{13/2}^{-1}$ bands in the odd-odd $^{184\text{–}194}$Au nuclei. It can be seen in this figure that all the bands display apparent signature splitting at low spins. Remarkably, the low-spin signature inversion phenomenon has been systematically observed in $^{184\text{–}192}$Au; i.e., the $\alpha_{uf} = 1$ sequence lies lower than the $\alpha_f = 0$ sequence at low spins. For ^{184}Au, the inversion spin is observed at $I^\pi = 16.5^-$. Both features of apparent signature splitting and signature inversion observed at low spins in band 7 of ^{184}Au provide supplementary arguments for the spin and configuration assignments for this band.

Figure 16(c) shows the reversion frequencies for the oblate $\pi h_{11/2}^{-1} \otimes \nu i_{13/2}^{-1}$ bands in the Au isotopes. Due to lack of higher spin data, no accurate reversion frequency can be extracted for ^{186}Au. One can see in Fig. 16(c) that the change of the reversion frequency versus the neutron number is not so regular. For ^{184}Au and ^{188}Au, the reversion frequency increases with increasing neutron number. However, for ^{188,190,192}Au, the reversion frequency decreases with increasing neutron number. Following the variation tendency, it is reasonable to speculate that the signature inversion might exist below $\hbar\omega = 0.207$ MeV in ^{194}Au, where $\hbar\omega = 0.207$ MeV corresponds to the first measured rotational frequency in the $\alpha = 0$ sequence of the $\pi h_{11/2}^{-1} \otimes \nu i_{13/2}^{-1}$ band [55]. In fact, the Routhians of the two signature sequences in the $\pi h_{11/2}^{-1} \otimes \nu i_{13/2}^{-1}$ band of ^{194}Au tend to cross with decreasing rotational frequency.

For the oblate $\pi h_{11/2}^{-1} \otimes \nu i_{13/2}^{-1}$ bands in $^{186\text{–}192}$Au, the low-spin signature inversion has been studied in the framework of the cranked shell model [13,54,57,59]; it has been documented that the triaxial deformation plays an important role in generating low-spin signature inversion. Furthermore, the theoretical reversion frequencies in ^{188,190}Au [54,57] were in excellent agreement with the experimentally measured ones. Since the oblate $\pi h_{11/2}^{-1} \otimes \nu i_{13/2}^{-1}$ bands have been observed only in a limited range of nuclei, the observation of the low-spin signature inversion in the $\pi h_{11/2}^{-1} \otimes \nu i_{13/2}^{-1}$ band of ^{184}Au provides an example for systematic and theoretical investigations. This study extends the knowledge of low-spin signature inversion for the oblate $\pi h_{11/2}^{-1} \otimes \nu i_{13/2}^{-1}$ configuration to the most neutron deficient odd-odd Au isotope.

IV. SUMMARY AND CONCLUSIONS

The present article presents the results of an in-beam study of high-spin states in deformed odd-odd ^{184}Au populated through the ^{159}Tb(^{29}Si, $4n\gamma$) reaction. With the help of the high detection sensitivity of the GASP multidetector array, a revised level scheme of ^{184}Au consisting of seven rotational bands and an irregular structure has been constructed. Apart from the much extended prolate $\pi h_{9/2} \otimes \nu 7/2^-[514]$, $\pi h_{9/2} \otimes \nu 1/2^-[521]$, $\pi h_{9/2} \otimes \nu i_{13/2}$, and $\pi i_{13/2} \otimes \nu i_{13/2}$ bands, three new rotational bands associated with prolate $\pi 1/2^+[660] \otimes \nu 7/2^-[514]$ and $\pi 11/2^-[505] \otimes \nu 7/2^-[514]$ and oblate $\pi h^{-1}_{11/2} \otimes \nu i^{-1}_{13/2}$ configurations, respectively, have been identified in this work. Configuration evolution from $\pi 3/2^-[532](h_{9/2}) \otimes \nu 7/2^-[514]$ to $\pi 1/2^-[541](h_{9/2}) \otimes \nu 7/2^-[514]$ with increasing spin has been proposed in the ground-state band of ^{184}Au. The band properties, such as band crossing frequencies, alignment gains, and signature splittings, have been discussed within the framework of the cranked shell model. Both $\pi h_{9/2}$ and $\nu i_{13/2}$ crossings have been observed in ^{184}Au. The level spins of the $\pi h_{9/2} \otimes \nu i_{13/2}$ band have been reassigned in this work, which leads to the observation of low-spin signature inversion in this band. Meanwhile low-spin signature inversion has also been established for the prolate $\pi i_{13/2} \otimes \nu i_{13/2}$ and oblate $\pi h^{-1}_{11/2} \otimes \nu i^{-1}_{13/2}$ bands in ^{184}Au. The present work extends our knowledge of shape coexistence, low-frequency $\pi h_{9/2}$ crossing, and low-spin signature inversion.

ACKNOWLEDGMENTS

The authors wish to thank the staffs at LNL-INFN, Italy, for providing the ^{29}Si beam during the experiment. This work was supported by the National Natural Sciences Foundation (Grants No. 11175217, No. 10825522, No. 11105186, and No. 10735010), the Major State Basic Research Development Program of China (Grant No. 2007CB815000), and the Chinese Academy of Sciences.

[1] R. Bengtsson, T. Bengtsson, J. Dudek, G. Leander, W. Nazarewicz, and J. Zhang, Phys. Lett. B **183**, 1 (1987).
[2] W. F. Mueller *et al.*, Phys. Rev. C **59**, 2009 (1999).
[3] A. J. Larabee, M. P. Carpenter, L. L. Riedinger, L. H. Courtney, J. C. Waddington, V. P. Janzen, W. Nazarewicz, J.-Y. Zhang, R. Bengtsson, and G. A. Lèander, Phys. Lett. B **169**, 21 (1986).
[4] J. Nyberg *et al.*, Nucl. Phys. A **511**, 92 (1990).
[5] F. Hannachi, G. Bastin, M. G. Porquet, J. P. Thibaud, C. Bourgeois, L. Hildingsson, N. Perrin, H. Sergolle, F. A. Beck, and J. C. Merdinger, Z. Phys. A **330**, 15 (1988).
[6] F. Ibrahim *et al.*, Phys. Rev. C **54**, 1547 (1996).
[7] V. P. Janzen *et al.*, Phys. Rev. Lett. **61**, 2073 (1988).
[8] S. Pilotte, G. Kajrys, S. Monaro, M. P. Carpenter, V. P. Janzen, L. L. Riedinger, J. K. Johansson, D. G. Popescu, D. D. Rajnauth, and J. C. Waddington, Phys. Rev. C **40**, 610 (1989).
[9] D. L. Balabanski, W. Gast, G. Hebbinghaus, A. Kramer-Flecken, R. M. Lieder, T. Morek, T. Rzaca-Urban, H. Schnare, and W. Urban, Z. Phys. A **332**, 111 (1989).
[10] M. Danchev *et al.*, Phys. Rev. C **68**, 054307 (2003).
[11] M. P. Carpenter *et al.*, Nucl. Phys. A **513**, 125 (1990).
[12] G. Hebbinghaus, W. Gast, A. Kramer-Flecken, R. M. Lieder, J. Skalski, and W. Urban, Z. Phys. A **328**, 387 (1987).
[13] V. P. Janzen *et al.*, Phys. Rev. C **45**, 613 (1992).
[14] J. K. Johansson, D. G. Popescu, D. D. Rajnauth, J. C. Waddington, M. P. Carpenter, L. H. Courtney, V. P. Janzen, A. J. Larabee, Z. M. Liu, and L. L. Riedinger, Phys. Rev. C **40**, 132 (1989).
[15] C. Bourgeois, M. G. Porquet, N. Perrin, H. Sergolle, F. Hannachi, G. Bastin, and F. Beck, Z. Phys. A **333**, 5 (1989).
[16] R. Bengtsson, H. Frisk, F. R. May, and J. A. Pinston, Nucl. Phys. A **415**, 189 (1984).
[17] G. García Bermúdez and M. A. Cardona, Phys. Rev. C **64**, 034311 (2001).
[18] Y. H. Zhang *et al.*, Eur. Phys. J. A **14**, 271 (2002).
[19] Y. H. Zhang *et al.*, Phys. Rev. C **68**, 054313 (2003).
[20] Ts. Venkova *et al.*, Eur. Phys. J. A **20**, 375 (2004).
[21] F. Ibrahim *et al.*, Z. Phys. A **350**, 9 (1994).
[22] J. Sauvage *et al.* (ISOLDE and NICOLE Collaborations), Eur. Phys. J. A **25**, 5 (2005).
[23] Y. H. Zhang *et al.*, Phys. Rev. C **70**, 057303 (2004).
[24] Y. H. Zhang *et al.*, Chin. Phys. Lett. **21**, 799 (2004).
[25] Y. H. Zhang *et al.*, J. Phys. G **31**, S1545 (2005).
[26] Y. H. Zhang *et al.*, Int. J. Mod. Phys. E **15**, 1437 (2006).
[27] L. T. Song *et al.*, Phys. Rev. C **71**, 017302 (2005).
[28] G. D. Dracoulis, B. Fabricius, T. Kibédi, A. P. Byrne, and A. E. Stuchbery, Nucl. Phys. A **554**, 439 (1993).
[29] F. Le Blanc *et al.* (ISOLDE Collaboration), Phys. Rev. Lett. **79**, 2213 (1997).
[30] A. J. Kreiner, J. Davidson, M. Davidson, D. Abriola, C. Pomar, and P. Thieberger, Phys. Rev. C **36**, 2309 (1987); **37**, 1338(E) (1988).
[31] C. J. Gallagher, Jr. and S. A. Moszkowski, Phys. Rev. **111**, 1282 (1958).
[32] F. Dönau and S. Frauendorf, in *Proceedings of the Conference on High Angular Momentum Properties of Nuclei, Oak Ridge, 1982*, edited by N. R. Johnson (Harwood Academic, New York, 1983), p. 143.
[33] D. Hojman *et al.*, Phys. Rev. C **67**, 024308 (2003); **78**, 029903(E) (2008).
[34] G. J. Lane, G. D. Dracoulis, A. P. Byrne, P. M. Walker, A. M. Baxter, J. A. Sheikh, and W. Nazarewicz, Nucl. Phys. A **586**, 316 (1995).
[35] R. Bengtsson and S. Frauendorf, Nucl. Phys. A **314**, 27 (1979).
[36] S. Drissi, A. Bruder, J.-Cl. Dousse, V. Ionescu, J. Kern, J.-A. Pinston, S. André, D. Barnéoud, J. Genevey, and H. Frisk, Nucl. Phys. A **451**, 313 (1986).
[37] F. Hannachi *et al.*, Nucl. Phys. A **481**, 135 (1988).
[38] R. A. Bark, A. M. Baxter, A. P. Byrne, P. M. Davidson, G. D. Dracoulis, S. M. Mullins, T. R. McGoram, and R. T. Newman, Phys. Rev. C **67**, 014320 (2003).
[39] Y. H. Zhang *et al.*, Eur. Phys. J. A **13**, 429 (2002).
[40] A. J. Kreiner, D. E. Di Gregorio, A. J. Fendrik, J. Davidson, and M. Davidson, Phys. Rev. C **29**, 1572 (1984).
[41] A. J. Kreiner, J. Davidson, M. Davidson, P. Thieberger, and E. K. Warburton, Phys. Rev. C **42**, 878 (1990).
[42] A. J. Kreiner, J. Davidson, M. Davidson, P. Thieberger, E. K. Warburton, S. André, and J. Genevey, Nucl. Phys. A **489**, 525 (1988).
[43] R. A. Bark *et al.*, Phys. Lett. B **406**, 193 (1997); **416**, 453(E) (1998).
[44] A. Aguilar *et al.*, Phys. Rev. C **81**, 064317 (2010).

[45] Y. H. Zhang, T. Hayakawa, M. Oshima, J. Katakura, Y. Hatsukawa, M. Matsuda, H. Kusakari, M. Sugawara, T. Komatsubara, and K. Furuno, Phys. Rev. C **65**, 014302 (2001).
[46] R. Bengtsson, Nucl. Phys. A **520**, 201c (1990).
[47] W. Nazarewicz, M. A. Riley, and J. D. Garrett, Nucl. Phys. A **512**, 61 (1990).
[48] P. Joshi, A. Kumar, G. Mukherjee, R. P. Singh, S. Muralithar, U. Garg, R. K. Bhowmik, and I. M. Govil, Phys. Rev. C **66**, 044306 (2002).
[49] P. Joshi, A. Kumar, I. M. Govil, R. P. Singh, G. Mukherjee, S. Muralithar, R. K. Bhowmik, and U. Garg, Phys. Rev. C **69**, 044304 (2004).
[50] F. G. Kondev, G. D. Dracoulis, A. P. Byrne, and T. Kibédi, Nucl. Phys. A **632**, 473 (1998).
[51] G. D. Dracoulis, S. M. Mullins, A. P. Byrne, F. G. Kondev, T. Kibédi, S. Bayer, G. J. Lane, T. R. McGoram, and P. M. Davidson, Phys. Rev. C **58**, 1444 (1998).
[52] H. M. El-Masri *et al.*, Phys. Rev. C **72**, 054306 (2005).
[53] S. C. Li *et al.*, Chin. Phys. Lett. **29**, 022102 (2012).
[54] Y. D. Fang *et al.*, Phys. Rev. C **82**, 064303 (2010); **83**, 019902(E) (2011).
[55] A. Neskakis, R. M. Lieder, H. Beuscher, Y. Gono, D. R. Haenni, and M. Müller-Veggian, Nucl. Phys. A **390**, 53 (1982).
[56] E. Gueorguieva *et al.*, Phys. Rev. C **64**, 064304 (2001).
[57] E. Gueorguieva, C. Schück, A. Minkova, Ch. Vieu, M. Kaci, F. Hannachi, R. Wyss, J. S. Dionisio, A. Korichi, and A. Lopez-Martens, Phys. Rev. C **69**, 044320 (2004).
[58] B. S. Gao *et al.*, Phys. Rev. C **86**, 054310 (2012).
[59] Y. Oktem *et al.*, Phys. Rev. C **86**, 054305 (2012).
[60] G. J. Lane, G. D. Dracoulis, A. P. Byrne, S. S. Anderssen, P. M. Davidson, B. Fabricius, T. Kibédi, A. E. Stuchbery, and A. M. Baxter, Nucl. Phys. A **589**, 129 (1995).
[61] M. Guttormsen, K. P. Blume, Y. K. Agarwal, A. v. Grumbkow, K. Hardt, H. Hübel, J. Recht, and P. Schüler, Z. Phys. A **312**, 155 (1983).
[62] D. Ye *et al.*, Nucl. Phys. A **537**, 207 (1992).
[63] N. Roy *et al.*, Phys. Rev. C **47**, 930(R) (1993).
[64] D. Mehta *et al.*, Z. Phys. A **339**, 317 (1991).
[65] W. F. Mueller, H. J. Jensen, W. Reviol, L. L. Riedinger, C.-H. Yu, J.-Y. Zhang, W. Nazarewicz, and R. Wyss, Phys. Rev. C **50**, 1901 (1994).
[66] S. Shastry, J. C. Bacelar, J. D. Garrett, G. B. Hagemann, B. Herskind, and J. Kownacki, Nucl. Phys. A **470**, 253 (1987).
[67] D. J. Hartley *et al.*, Phys. Rev. C **65**, 044329 (2002).
[68] S. C. Li *et al.*, Sci. Sin-Phys. Mech. Astron. **42**, 1062 (2012).
[69] M. A. Cardona *et al.*, Phys. Rev. C **66**, 044308 (2002).
[70] G. Zhao, Y. Liu, J. Lu, Y. Ma, L. Yin, X. Li, Z. Li, X. Wu, G. Li, S. Wen, and C. Yang, Eur. Phys. J. A **9**, 299 (2000).
[71] S. K. Katoch, S. L. Gupta, S. C. Pancholi, D. Mehta, S. Malik, G. Shanker, L. Chaturvedi, and R. K. Bhowmik, Eur. Phys. J. A **4**, 307 (1999).
[72] S. X. Wen (unpublished).
[73] G. Levinton *et al.*, Phys. Rev. C **60**, 044309 (1999).
[74] Y. H. Zhang *et al.*, Phys. Rev. C **60**, 044311 (1999).
[75] D. Hojman *et al.*, Phys. Rev. C **61**, 064322 (2000).
[76] S. Guo *et al.*, Phys. Rev. C **86**, 014323 (2012).
[77] M. A. Cardona *et al.*, Phys. Rev. C **59**, 1298 (1999).